Acta Pharmaceutica Sinica B 2022;12(1):210–227

Chinese Pharmaceutical Association
Institute of Materia Medica, Chinese Academy of Medical Sciences

Acta Pharmaceutica Sinica B

www.elsevier.com/locate/apsb
www.sciencedirect.com

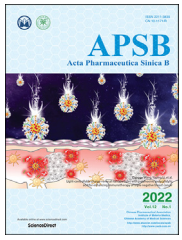

ORIGINAL ARTICLE

The novel ER stress inducer Sec C triggers apoptosis by sulfating ER cysteine residues and degrading YAP *via* ER stress in pancreatic cancer cells

Junxia Wang[†], Minghua Chen[†], Mengyan Wang, Wenxia Zhao, Conghui Zhang, Xiujun Liu, Meilian Cai, Yuhan Qiu, Tianshu Zhang, Huimin Zhou, Wuli Zhao[*], Shuyi Si[*], Rongguang Shao[*]

Key Laboratory of Antibiotic Bioengineering, Ministry of Health, Laboratory of Oncology, Institute of Medicinal Biotechnology, Chinese Academy of Medical Sciences and Peking Union Medical College, Beijing 100050, China

Received 8 February 2021; received in revised form 11 June 2021; accepted 16 June 2021

KEY WORDS

Pancreatic cancer;
Secoemestrin C;
YAP degradation;
ER stress inducer;
Resistance;
Fast shrinkage;
YAP destruction complex;
Lipid droplet formation

Abstract Pancreatic adenocarcinoma (PAAD) is one of the most lethal malignancies. Although gemcitabine (GEM) is a standard treatment for PAAD, resistance limits its application and therapy. Secoemestrin C (Sec C) is a natural compound from the endophytic fungus *Emericella*, and its anticancer activity has not been investigated since it was isolated. Our research is the first to indicate that Sec C is a broad-spectrum anticancer agent and could exhibit potently similar anticancer activity both in GEM-resistant and GEM-sensitive PAAD cells. Interestingly, Sec C exerted a rapid growth-inhibiting effect (80% death at 6 h), which might be beneficial for patients who need rapid tumor shrinkage before surgery. Liquid chromatography/mass spectrometry and *N*-acetyl-L-cysteine (NAC) reverse assays show that Sec C sulfates cysteines to disrupt disulfide-bonds formation in endoplasmic reticulum (ER) proteins to cause protein misfolding, leading to ER stress and disorder of lipid biosynthesis. Microarray data and subsequent assays show that ER stress-mediated ER-associated degradation (ERAD) ubiquitinates and

*Corresponding authors. Tel.: +86 10 83166673.
E-mail addresses: wenlyzh@imb.pumc.edu.cn (Wuli Zhao), sisyimb@hotmail.com (Shuyi Si), rgshao@163.com (Rongguang Shao).
[†]These authors made equal contributions to this work.
Peer review under responsibility of Chinese Pharmaceutical Association and Institute of Materia Medica, Chinese Academy of Medical Sciences.

https://doi.org/10.1016/j.apsb.2021.07.004

downregulates YAP to enhance ER stress *via* destruction complex (YAP−Axin−GSK−βTrCP), which also elucidates a unique degrading style for YAP. Potent anticancer activity in GEM-resistant cells and low toxicity make Sec C a promising anti-PAAD candidate.

1. Introduction

Pancreatic cancer is one of the most refractory and aggressive digestive system cancers and has a low resection rate. Pancreatic ductal adenocarcinoma is the most common type of pancreatic cancer[1]. Despite advances in diagnosis and treatment, survival rates of pancreatic adenocarcinoma (PAAD) have not changed significantly in the past two decades; the 5-year survival rate remains lower than 5%[1,2]. Surgical resection is the primary treatment for this cancer. However, due to a lack of significant symptoms and effective tumor biomarkers, relatively few diagnosed patients can undergo initial resection before progression of the disease to the advanced stage[3]. Therefore, drug treatment has become a vital modality for patients with advanced unresectable metastatic cancer. Gemcitabine is the standard first-line drug for pancreatic cancer treatment. Although GEM is effective in some pancreatic cancer patients[4], many patients exhibit primary or secondary resistance to it, which limits pancreatic cancer treatment. As reported in the literature[5−7], many cell lines such as MIA PaCa2, PANC-1, SU86.86 and SW 1990 are gemcitabine (GEM)-resistant (GEM-R); the IC_{50} of GEM in these cells is much higher than the IC_{50} in GEM-sensitive (GEM-S) cells such as AsPC-1 and BxPC-3 cells. For GEM-R pancreatic cancers, the use of second-line therapies such as combined administration of several chemotherapy drugs, has not obviously improved the survival rate[8]. Furthermore, the relatively high toxicity of second-line anticancer drugs that are commonly used for other clinical tumor applications tends to increase the pain of the patients; thus, it is necessary to investigate novel and low-toxicity antipancreatic cancer drugs for GEM-R patients.

At present, many anticancer drugs are targeted drugs. The targets are usually specific proteins or molecules; relatively few drugs target organelles or other cellular components, except for DNA-targeting agents. However, many organelles such as the membranous endoplasmic reticulum (ER) are necessary for cell survival, especially in tumor cells. The ER is the primary subcellular organelle responsible for the synthesis, transport, and posttranslational modification of proteins and for the biosynthesis of lipids and sterols in eukaryotic cells[9−11]. Loss of ER homeostasis perturbs the biosynthesis of proteins and lipids that are necessary for cell survival. The ER is particularly important in pancreatic tissue because the pancreas is a digestive organ, and most digestion-promoting proteins/enzymes are produced by the pancreatic ER; thus, compared with ER in other cell types, the ER in pancreatic cells is particularly well developed, especially the rough ER[12−14].

In tumors, abnormal proliferation requires elevated protein synthesis and increased levels of nutrients; correspondingly, hypoxia and nutrient deprivation are induced[11,15,16]. These changes trigger the unfolded protein response (UPR), which helps cells adapt to stress to restore ER homeostasis. However, if cells are unable to overcome ER damage, cell death mediated by ER stress responses may become dominant and lead to tumor cell apoptosis[11,17]. In the ER, cysteine residues are abundant, especially in cancer, and targeting and sulfurizing ER cysteine could disrupt thiol proteostasis to block the normal disulfide bond of ER proteins to inhibit cancer growth[18]. Therefore, therapeutic strategies aimed at targeting ER cysteine residues and inducing the ER stress response could be beneficial for anticancer treatments. By increasing ER-stress and manipulating ER homeostasis to promote the proapoptotic pathway, drug investigation has been performed. In particular, some studies have found that secretory cancer cells are more sensitive to ER stress than normal cells, suggesting that targeting ER in pancreatic cancer cells might be a beneficial strategy for pancreatic cancer treatment[11,17].

Natural antitumor compounds such as paclitaxel and doxorubicin have been found to play dominant roles in the treatment of human tumors. Compared with natural products from plants and marine organisms[19], natural products from endophytic fungi are more plentiful and have shorter regeneration cycles. In addition, industrial fermentation of endophytic fungi can be conducted on a large scale at a low cost and is pollution-free. In recent years, many endophytic fungal products have been isolated and applied widely for tumor treatment. For instance, Taxol was originally isolated from the secondary metabolites of endophytic fungi, and vinblastine analogs have been isolated from the secondary metabolites of periwinkle endophytic fungi. Our research team has been exploring natural compounds derived from endophytic fungi and obtained a library of natural product extracts through microbial fermentation. After screening the antitumor activity of these extracts, we obtained an anticancer compound (Fig. 1A, purity 98%, from rice fermentation of *Emericella* sp.) with potent activity against several tumor cell lines derived from different tissues, and the IC_{50} is displayed in Supporting Information Fig. S1A.

Upon searching the literature, we found only a few papers mentioning this compound, called secoemestrin C (Sec C), which was first isolated in 1997. To date, only limited data have reported its kinase-associated activity, but the anticancer activity of Sec C has not been reported[20]. By analyzing the IC_{50} of Sec C on various tumor cells, we found either in GEM-S pancreatic cancer cells or in GEM-R pancreatic cancer cells, Sec C all exhibited potent and similar anticancer activity. As mentioned above, compared with tumors derived from other tissues, drug treatment is more vital for pancreatic cancer due to untimely resection, and primary or secondary resistance to GEM limits pancreatic cancer treatment. Thus, we first focused on the anticancer effect of Sec C on pancreatic cancer.

In this study, we obtained the first evidence that the natural fungal compound Sec C can exhibit potent anticancer effects in various tumor cell lines. We found that Sec C also exerts similar excellent inhibitory effects in GEM-R pancreatic cancer cells,

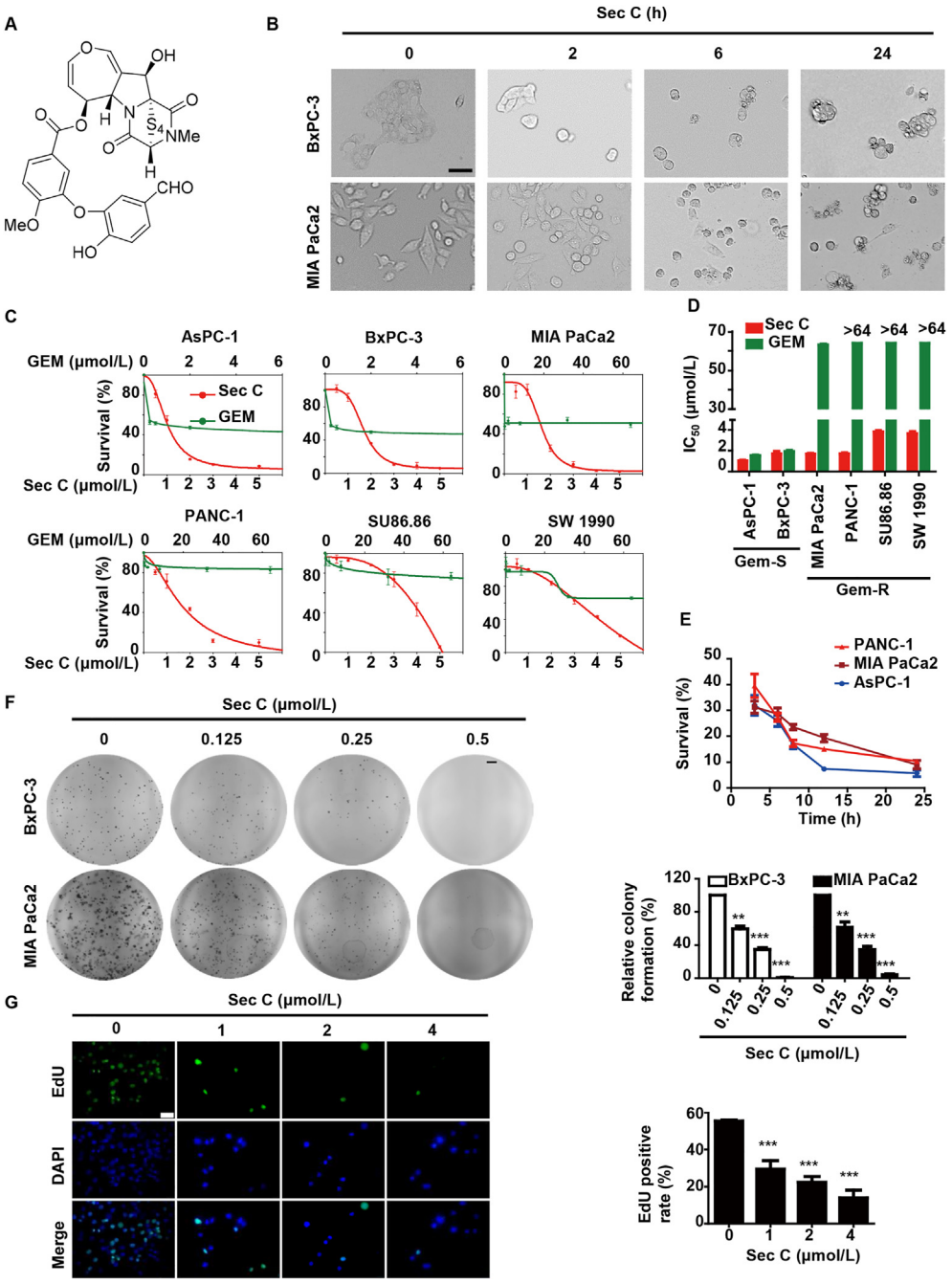

Figure 1 Sec C exhibits potent antipancreatic cancer activity that is similar in GEM-S and GEM-R pancreatic cancer cells. (A) Chemical structure of Sec C. (B) The cell morphology of BxPC-3 and MIA PaCa2 cells was observed after treatment with 3 μmol/L Sec C for the indicated time points. Scale bar, 12.5 μm. (C) Different pancreatic cancer cells were treated with the indicated concentrations of Sec C or GEM for 48 h, and cell survival was detected with MTT assay. A dose-dependent curve was plotted using SigmaPlot software. (D) IC_{50} of Sec C and gemcitabine in different pancreatic cancer cell lines. (E) Vitality of AsPC-1, MIA PaCa2 and PANC-1 cells was determined by MTT assay after treatment with 3 μmol/L Sec C for the indicated time points. A time-dependent curve was plotted. (F) BxPC-3 and MIA PaCa2 cells were seeded in 6-well plates at 2000 cells. After 24 h, various concentrations of Sec C were added and continued to incubate for 7 days. Then visible colonies were counted as described in section of Materials and methods. Colony formation rate (%)=(numbers of colonies/numbers of seeded cells) × 100. Scale bar, 3 mm. (G) MIA PaCa2 cells were treated with different concentrations of Sec C for 24 h, and cell proliferation was detected with EdU assay. Scale bar, 40 μm. The data are shown as mean ± SEM ($n = 3$); $^{*}P < 0.05$, $^{**}P < 0.01$, $^{***}P < 0.001$ *vs.* 0 μmol/L group.

indicating that Sec C could overcome GEM resistance. In addition, Sec C killed cancer cells rapidly (in 6 h treatment, 80% of cells died). A mechanistic study showed that Sec C could form a disulfide bond with ER proteins to disturb thiol proteostasis to induce dysregulation of disulfide bond formation in ER proteins, leading to ER stress and apoptosis. In addition, YAP degradation plays an essential role in the aggravation of ER damage by ER stress-mediated ubiquitylation and proteasomal degradation,

further revealing a unique role of YAP that differs from the previously reported roles of YAP in ER stress.

2. Materials and methods

2.1. Reagents

GEM was purchased from the Cancer Hospital of the Chinese Academy of Medical Sciences (Beijing, China). Anti-PARP, anti-cleaved PARP, anti-caspase 3, anti-cleaved caspase 3, anti-GAPDH, anti-cytochrome *c*, anti-COX IV, anti-BCL2, anti-PUMA, anti-BIP, anti-BAX, anti-YAP, anti-ubiquitin, anti-β-TrCP, anti-AXIN1, and anti-GSK3β antibodies were purchased from Cell Signaling Technology (Danvers, MA, USA). Anti-EIF2α, anti-phospho-EIF2α (Ser51), anti-ATF4, anti-IRE1α, anti-phospho-IRE1α, anti-XBP1, anti-ATF6, anti-phospho-JNK, anti-JNK antibodies and an Annexin V-FITC apoptosis detection kit were purchased from Beyotime (Jiangsu, China). Peroxidase-conjugated goat antimouse and goat antirabbit secondary antibodies were purchased from ZSGQ-BIO Company (Beijing, China). A Cell-Light 5-ethynyl-2′-deoxyuridine (EdU) kit was purchased from RiboBio Company (Guangzhou, China). A mitochondrial staining kit and a kit for 1,3,5,7-tetramethyl-8-phenyl-4,4-difluoroboradiazaindacene (BODIPY) staining of lipid droplets were purchased from Thermo Fisher Scientific Inc. (Waltham, MA, USA). MTT, cycloheximide (CHX), MG132 and bafilomycin (BAF) were purchased from Sigma−Aldrich (St. Louis, MO, USA). *BIP* siRNA and *YAP* siRNA were purchased from Santa Cruz Biotechnology Inc. (Santa Cruz, CA, USA). *N*-Acetylcysteine (NAC) was purchased from Selleck Chemicals (Houston, TX, USA). Lipofectamine 2000 reagent was purchased from Invitrogen (Waltham, MA, USA). Real-time PCR master mix was purchased from Roche (Indianapolis, IN, USA).

2.2. Cell culture

AsPC-1, BxPC-3, MIA PaCa2, PANC-1, SW 1990 and SU86.86 human pancreatic cancer cells and Bel7404, AsPC-1, HCT116, HepG2, H1975, A549, H1299 and SKOV3 cells were obtained from the Institute of Basic Medical Sciences, Chinese Academy of Medical Sciences (Beijing, China) or our laboratory and cultured in DMEM or 1640 supplemented with 10% fetal bovine serum and 1% antibiotics in an incubator at 37 °C with 5% CO_2.

2.3. Plasmids, transient transfection and establishment of a stable cell line

pCMV3-YAP was purchased from Sino Biological Company (Beijing, China). YAP mutants (S127A, in which Ser127 of YAP was not phosphorylated, and S127D, in which Ser127 of YAP was consecutively phosphorylated) were constructed with a mutation kit from TransGen Biotech Company (Beijing, China). For transfection, cells (2×10^5 cells/well) were seeded in 6-well plates and transfected with plasmids the next day using Lipofectamine 2000 according to the manufacturer's instructions. pLV-ER-GFP was obtained as a gift from Pantelis Tsoulfas (Addgene plasmid #80069; http://n2t.net/addgene: 80069; RRID: Addgene_80069). pAcGFP-C1-Sec61β was obtained as a gift from Eric Schirmer (Addgene plasmid #62008; http://n2t.net/addgene: 62008; RRID: Addgene_62008). To generate PANC-1 cells stably expressing ER-GFP or Sec61-GFP, PANC-1 cells were transfected with pLV-ER-GFP or pAcGFP-C1-Sec61β plasmids for 24 h, and cells successfully transfected with the constructs were selected using G418 (2 mg/mL). PANC-1-ER and PANC-1-SEC61 polyclonal cells were maintained in complete DMEM containing G418 (1 mg/mL).

2.4. Cell growth inhibition assay

MTT was used to analyze cellular viability. A total of 5000−8000 cells per well were cultured in a 96-well plate at 37 °C with 5% CO_2. At the indicated time points following the addition of Sec C, 25 μL of MTT solution (2 mg/mL) was added to 75 μL of complete medium, and the cells were incubated for 4 h at 37 °C with 5% CO_2. Subsequently, the cell medium was discarded, and 150 μL DMSO was added to the wells. The absorbance was read at 490 nm. Growth inhibition (%) was calculated at each concentration, and the IC_{50} values were calculated by SigmaPlot.

2.5. Colony formation assay

A cell colony formation assay was performed as described previously[21]. Briefly, BxPC-3 or MIA PaCa2 cells were seeded in a 6-well plate at 2000 cells per well and treated with different concentrations of Sec C for 7 days. Then, the cells were washed with PBS, fixed with 2% paraformaldehyde for 15 min at room temperature, stained with a 0.1% crystal violet solution for 10 min, and washed three times with sterile water. Then, images of each well were obtained, and the individual clone types were identified.

2.6. EdU proliferation assay

MIA PaCa2 cells were treated with 1−4 μmol/L Sec C for 24 h, following standard protocols with EdU to detect active DNA synthesis as previously described[21]. Images were obtained using a Leica SP2 confocal microscope (Leica Microsystems, Exton, PA, USA) and analyzed with Leica confocal software. Five microscope views from each sample were counted and averaged.

2.7. Detection of apoptotic cells by flow cytometry

BxPC-3 and MIA PaCa2 cells were treated with 0, 2 and 4 μmol/L Sec C for 24 h, washed three times with PBS and collected for an Annexin V-FITC/propidium iodide staining assay. The assay was performed based on the protocol provided with the Cell Apoptosis Detection Kit. In brief, cells were resuspended in 195 μL of 1 × Annexin V binding buffer, and then 10 μL of Annexin V-FITC and 5 μL of propidium iodide were added to cells in turn. The cells were incubated for 20 min in the dark at room temperature. A BD FACSCalibur flow cytometer (BD Biosciences, San Jose, CA, USA) was used to measure apoptosis.

2.8. Mitochondrial potential detection

To observe the mitochondrial potential, 5,5′,6,6′-tetrachloro-1,1′,3,3′-tetraethylbenzimidazolylcarbocyanine, iodide (JC-1, Sigma−Aldrich) staining was used. JC-1 (10 mg/mL) was added to the medium, and BxPC-3 and MIA PaCa2 cells were incubated for 10 min at 37 °C in the dark to label the mitochondria. JC-1 aggregates showed red fluorescence, and JC-1 monomers showed green fluorescence. JC-1 monomers and JC-1 aggregates were detected with a BD FACSCalibur flow cytometer or a Leica SP2 confocal microscope (Leica Microsystems, Exton, PA, USA).

2.9. Immunoprecipitation and Western blot analysis

Cells were washed with PBS, and protein was extracted in coimmunoprecipitation buffer. Total cell lysates were immunoprecipitated with the appropriate antibodies overnight at 4 °C and then incubated with Protein A/G Plus Agarose (Santa Cruz, CA, USA) for 2 h at 4 °C. After three washes at 4 °C, the immunocomplexes were mixed with 2 × SDS loading buffer and boiled for 10 min. Equal amounts of coprecipitates or lysates were electrophoresed by SDS-PAGE and transferred to PVDF membranes. The membranes were blocked with 5% skimmed milk at room temperature for 1 h and then immunoblotted overnight with primary antibodies. The membranes were subsequently incubated for 2 h with an appropriate secondary antibody. The immunoreactive signals were revealed using the enhanced chemiluminescence method (Sigma−Aldrich) and visualized with a Protein Simple FluorChem HD2 imaging system (ProteinSimple, CA, USA).

2.10. BODIPY staining for lipid droplets

PANC-1 and AsPC-1 cells were treated with different concentrations of Sec C for 24 h and then washed three times with PBS. The cells were fixed with 2% paraformaldehyde for 15 min at room temperature and incubated with BODIPY and Hoechst together for 30 min at room temperature in the dark. The cells were washed with PBS three times and observed with a Leica SP2 confocal microscope (Leica Microsystems, Exton, PA, USA).

2.11. RNA sequencing (RNA-seq)

RNA of Sec C-treated and untreated cells was extracted based on the procedures of the RNA extraction kit (Invitrogen). Quality control of the raw reads enabled the downstream analysis to be based on clean reads with high quality. Sequencing was performed on a BGISEQ-500RS platform. The raw sequencing data are available in the Sequence Read Archive database in connection with BioProject F19FTSNCWLJ7274.

The clean reads were mapped to the reference genome using software HISAT2 (v2.0.4). Software Bowtie (v2.2.5) was applied to align the clean reads to the reference coding gene set, and the gene expression levels were calculated with software RSEM (v1.2.12). A heatmap was drawn with pheatmap (v1.0.8) according to the gene expression in different samples. Differential expression analysis was performed using the PossionDis function with thresholds of a false discovery rate (FDR) $\leq$ 0.001 and a $|\log2\ \text{Ritio}| \geq 1$. To gain insight into changes in phenotype, Gene Ontology (GO; https://www.geneontology.org) and Kyoto Encyclopedia of Genes and Genomes (KEGG; https://www.kegg.jp/) enrichment analyses of annotated differentially expressed genes (DEGs) were performed with Phyper based on a hypergeometric test. The significance levels for terms and pathways were corrected by Q values with a rigorous threshold (Q value $\leq$ 0.05) *via* the Bonferroni method.

2.12. Real-time PCR

Total RNA was isolated with TRIzol reagent (Invitrogen), while cDNA was generated using a Transcriptor First Strand cDNA Synthesis Kit (Roche). The relative expression levels of specific genes were determined with an ABI 7500 Fast Real-Time PCR system. The results were analyzed using the comparative ΔΔCt method. The primer sequences used for q-PCR were as follows: adipocyte lipid-binding protein 2 (*AP2*) forward, 5′-TACTGGGCCAGGAATTTGAC-3′; *AP2* reverse, 5′-GTGGAAGTGACGCCTTTCAT-3′; fat-inducing transcript 2 (*FIT2*) forward, 5′-TCACTCCTTCCTGCTGACCT-3′; *FIT2* reverse, 5′-AACCAAACAAGGTGCCAAAC-3′; fat-specific protein 27 (*FSP27*) forward, 5′-GCCCGTGTAACGTTTGATCT-3′; *FSP27* reverse, 5′-GAGGAGCTGCTGCAGGTAAC-3′; *YAP* forward, 5′-TTTCTCCTGGGACACTGACC-3′; *YAP* reverse, 5′-TCTTTGCCATCTCCCAACCT-3′; *GAPDH* forward, 5′-GCAAATTCCATGGCACCGT-3′; and *GAPDH* reverse, 5′-TCGCCCCACTTGATTTTGG-3′.

2.13. ER extraction

MIA PaCa2 cells were treated with 2 μmol/L Sec C for 24 h, and then the ER fraction was extracted following the Endoplasmic Reticulum Isolation Kit protocol (Sigma−Aldrich). Briefly, cells were homogenized in ice-cold homogenization buffer. The homogenates were centrifuged at 1000×*g* for 10 min, and the lipid layer was removed. Then, centrifugation at 12,000×*g* for 15 min was performed, and the lipid layer was removed. This supernatant fraction, which is the postmitochondrial fraction, is the source for microsomes. Then, postmitochondrial fraction was precipitated with calcium chloride to isolate rough ER-enriched microsomes. The sample was centrifuged at 8000×*g* for 10 min, the supernatant was removed, and the pellet was collected (enriched rough ER microsomes). All procedures were performed at 4 °C.

2.14. Fluorescence labeling of protein thiol groups by dibromobimane (dBrB) assay

The assay was performed as described in the literature by Seo et al.[18]. Briefly, MIA PaCa2 cells were exposed to the indicated doses of Sec C for 24 h, cells were collected, and ER was extracted and sonicated. Then, the samples were immediately reacted with 1.5 mol/L perchloric acid and incubated for 5 min on ice to precipitate the proteins. Next, the pelleted proteins were solubilized and neutralized, and the prepared proteins (1 μg) were mixed with 1 μmol/L dibromobimane (Sigma−Aldrich) and incubated for 40 min at 37 °C. Dibromobimane-bound protein-SH groups were measured, and fluorescence was normalized to the total protein levels and expressed as the percentage of protein-SH levels.

2.15. Analysis of Sec C-protein binding sites based on liquid chromatography tandem mass spectrometry (LC−MS/MS)

MIA PaCa2 cells were treated with Sec C (2 μmol/L) for 24 h, the ER fraction was extracted using an ER isolation kit, and mass spectrometric analysis of tryptic peptides was performed on a Q Exactive™ Hybrid Quadrupole-Orbitrap™ Mass Spectrometer (Thermo Fisher Scientific, USA). Peptides were sequenced by online microcapillary LC−MS/MS operated in a data-dependent mode, and tryptic peptides were identified using the Byonic program. The capillary column was made from a piece of 150-μm i.d. fused silica line with an internal frit that was in-house made. The column was packed with a reversed-phase ReproSil-Pur C18-AQ resin (3 μm, 120 Å, Dr. Maisch GmbH, Germany). The LC gradient was from 6% to 9% B for 5 min, from 9% to 14% B for 15 min, from 14% to 30% B for 30 min, from 30% to 40% B for 8 min and from 40% to 95% B for 2 min. Solvent A: 0.1% formic acid and 2% acetonitrile in water; B: 20% 0.1% formic acid in

acetonitrile. The flow rate was 600 nL/min. Ion intensity data were obtained from mass spectra generated using LC−MS/MS.

2.16. Antitumor activity of Sec C in vivo

Female BALB/C nude mice (18 ± 1 g) were obtained from SPF Biotechology Co., Ltd. (Beijing, China). The care and treatment of the experimental animals were conducted in accordance with the institutional guidelines at the Experimental Animal Center of the Chinese Academy of Medical Sciences. As described previously, MIA PaCa2 cells were injected subcutaneously (10^7 cells/tumor) into the right axillae of nude mice. Tumor-bearing mice were randomly divided into 3 groups ($n = 5$) when the tumor size reached approximately 80 mm^3. Sec C (2.5 mg/kg or 5 mg/kg) or GEM (50 mg/kg) was administered by intraperitoneal injection every two days until the tumor size in the negative control group was approximately 1000 mm^3. The mice were weighed, and the tumor width (W) and length (L) were measured with Vernier calipers every two days. Tumor volume was estimated based on Eq. (1):

$$V = 0.5 \times L \times W \times W \quad (1)$$

The animals were killed 18 days after administration, and the tumors were extracted and weighed.

2.17. Statistical analysis

The results are presented as the mean ± standard error of mean (SEM). One-way analysis of variance and Student's t-test were used to analyze the differences of means, and $P < 0.05$ was regarded as the threshold for statistical significance.

3. Results

3.1. Sec C exhibits potent anti-pancreatic cancer activity in GEM-R and GEM-S pancreatic cancer cells

Although GEM is widely used in pancreatic cancer treatment, its success is limited by resistance, which is observed in many patients with pancreatic cancer. In our anticancer activity screening of fungal metabolites, we found that compound Sec C exhibited strong anticancer activity in different tissue-derived cancer cells (Fig. S1A), although its anticancer activity has not been reported since it was isolated in 1997. Meanwhile, we observed that Sec C displayed similarly strong anticancer effects in GEM-R and GEM-S pancreatic cancer cells. As shown in Fig. 1B and Fig. S1B, Sec C exhibited potent anticancer effects in GEM-S pancreatic cancer cells and GEM-R cells. Morphological observation revealed that both GEM-S and GEM-R cells became round after treatment for 2 h with 3 μmol/L Sec C (approximately 1.5−2 times the IC_{50}); after 6 h, more than 80% of cells became nonadherent, lost their regular spindle shapes and became round, suggesting that the pancreatic cancer cells were nonviable (Fig. 1B and Fig. S1B). Further survival detection by trypan staining verified this hypothesis. We also investigated the effects of GEM on GEM-R/S cells under the same treatment conditions as those used for Sec C (6 h treatment at a dose of 2 times the IC_{50} of GEM) and found that GEM did not induce obvious morphological changes. The MTT assay results also supported this observation, revealing that 85% of cells remained alive at the end of treatment (data not shown). These findings suggest that Sec C is an anticancer agent characterized by rapid efficacy.

To evaluate the dose-dependent effects of Sec C, 0, 0.5, 1.0, 2.0, 3.0 and 5.0 μmol/L Sec C were added to 2 types of GEM-S pancreatic cancer cells (BxPC-3 and AsPC-1 cells) and 4 types of GEM-R pancreatic cancer cells (MIA PaCa2, PANC-1, SW 1990 and SU86.86 cells) for 48 h, and cell viability was examined. The results show that for both GEM-S and GEM-R cells, Sec C significantly inhibited cell growth in a dose-dependent manner (Fig. 1C). For instance, with regard to AsPC-1, after Sec C treatment for 48 h, cell survival rate was about 97% of control at 0.5 μmol/L and decreased to about 75% at 1.5 μmol/L (Fig. 1C). And when the concentration was up to 3 μmol/L, the survival rate was only 10% of control, indicating an obvious dose-dependent manner. Correspondingly, we also observed a similar dose-dependent effect of Sec C in other pancreatic cancer cell types and obtained the IC_{50} according to a survival rate−concentration curve (Fig. 1C).

We also detected the effects of GEM on the abovementioned GEM-S/GEM-R pancreatic cancer cells and obtained results similar to the results reported in the literature (Fig. 1C)[5−7]. Upon comparing the IC_{50} between GEM and Sec C, we found that for GEM-S cells, the IC_{50} of Sec C was similar to the IC_{50} of GEM (approximately 1−2 μmol/L) (Fig. 1C and D). For GEM-R cells, Sec C still displayed excellent anticancer effects, and the IC_{50} values of Sec C in GEM-R cells and GEM-S cells were similar. However, the GEM IC_{50} in GEM-R cells was greater than 64 μmol/L (Fig. 1C and D), and it was 16-fold higher than the IC_{50} of Sec C, indicating that Sec C exhibits good inhibitory effects regardless of GEM resistance and can in fact abrogate resistance.

The time-dependent effect of Sec C was investigated at 3, 6, 9, 12 and 24 h (Fig. 1E). Among AsPC-1 cells, approximately 68% of cells were viable after 3 h, while 8% and 7.5% of cells were viable after 12 and 24 h, respectively. Among MIA PaCa2 cells treated with 3 μmol/L Sec C, the cell viability rates were 72%, 8% and 3% of the control rates at 3, 14 and 24 h, respectively (Fig. 1E). Other types of cells also exhibited similar time-dependent effects (Fig. 1E).

Given that colony formation analysis is the gold standard method for the analysis of agent cytotoxicity, we utilized colony formation assays to further assess the inhibitory effects of Sec C. BxPC-3 cells and MIA PaCa2 cells were seeded in 6-well plates and incubated with increasing concentrations of Sec C (0, 0.125, 0.25 and 0.5 μmol/L) for 7 days before colony counting. The results showed that Sec C inhibited the colony formation of tumor cells in a dose-dependent manner. At 0.125 μmol/L, the colony formation rate of treated cells was approximately 60% of the colony formation rate of control cells. In addition, the colony formation rate of 0.25 μmol/L Sec C-treated cells was approximately 25% of the colony formation rate of control cells, while the rate of 0.5 μmol/L Sec C-treated cells was approximately 0% of the colony formation rate of control cells. These findings indicated an obvious dose-dependent inhibitory effect in both GEM-S and GEM-R pancreatic cancer cells (Fig. 1F).

EdU, which is similar in structure to a component of DNA, is incorporated into DNA during active DNA synthesis and enables easy visualization of DNA replication[22]. We used an EdU assay to examine the effect of Sec C on DNA replication and found that the EdU-positive cell rate decreased with increasing Sec C concentrations (Fig. 1G), indicating a strong and dose-dependent effect of Sec C on DNA replication.

All these findings indicate that Sec C, a natural metabolite derived from fungi, has similar strong inhibitory effects on GEM-R and GEM-S pancreatic cancer cells, suggesting that Sec C potently reverses GEM resistance. Additionally, this compound can induce rapid tumor cell death, which will be beneficial for patients in urgent need of tumor shrinkage before further treatment.

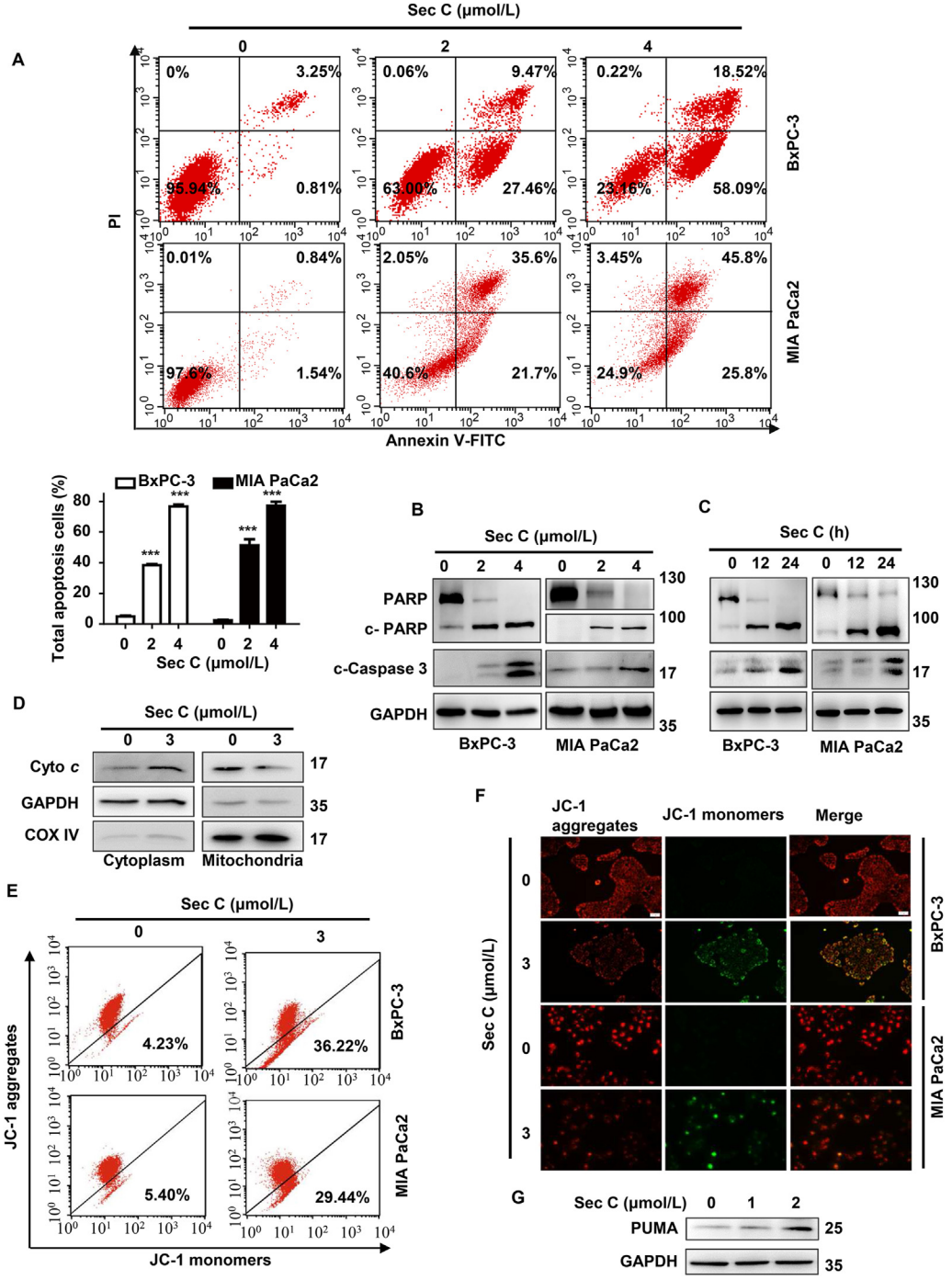

Figure 2 Sec C induces mitochondria-mediated apoptosis in GEM-S and GEM-R pancreatic cancer cells. (A) BxPC-3 and MIA PaCa2 cells were treated with 0, 2 or 4 μmol/L Sec C for 24 h, and cells were stained with propidium iodide and Annexin V-FITC for flow cytometry detection. The data are shown as mean ± SEM ($n = 3$); ***$P < 0.001$ *vs.* 0 μmol/L group. (B) BxPC-3 and MIA PaCa2 cells were treated with different concentrations of Sec C for 24 h, and apoptosis-associated proteins were detected by immunoblotting. (C) BxPC-3 and MIA PaCa2 cells were treated with 3 μmol/L Sec C for the indicated time points, and apoptosis-associated proteins were detected by immunoblotting. (D) BxPC-3 cells were treated with Sec C for 24 h, and cytoplasm and mitochondria were isolated. Cytochrome *c* was determined by immunoblotting. BxPC-3 and MIA PaCa2 cells were treated with Sec C for 24 h, and then cells were stained with JC-1 for flow cytometry detection (E) and fluorescence microscopy detection (F; scale bar, 50 μm). (G) PUMA protein levels were detected after MIA PaCa2 cells were treated with Sec C for 24 h.

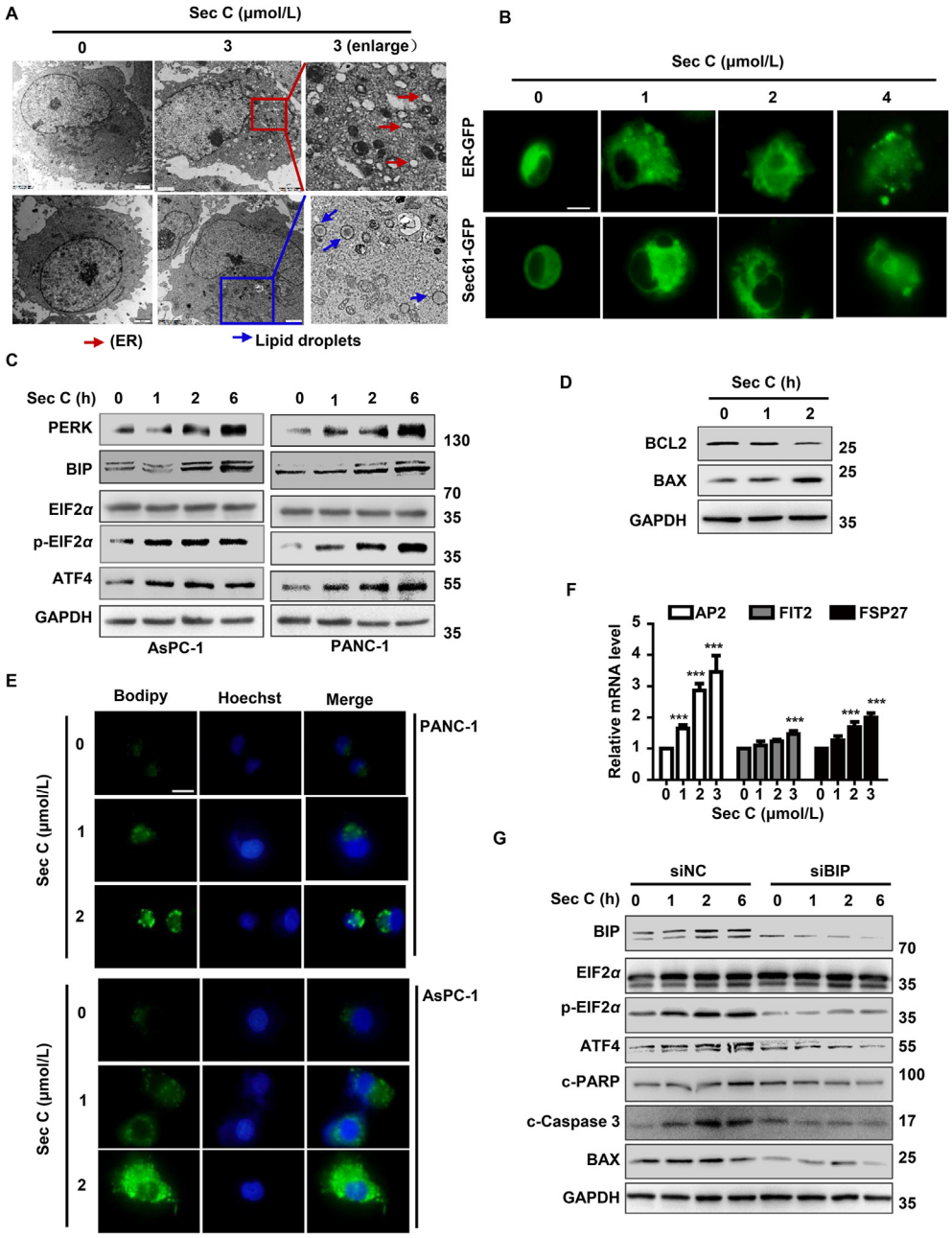

Figure 3 Sec C induces ER stress and lipid droplet formation in GEM-R and GEM-S cells. (A) After treatment with 3 μmol/L Sec C for 24 h, MIA PaCa2 cells were observed with transmission electron microscopy. ER vacuolation (red arrow) and lipid droplets (blue arrow). (B) PANC-1 cells stably expressing ER-GFP/SEC61-GFP (ER-localized protein) were treated with different concentrations of Sec C for 6 h, and representative images were acquired with a confocal microscope. Scale bar, 20 μm. (C) AsPC-1 and PANC-1 cells were incubated with 3 μmol/L Sec C for the indicated time points, and ER stress-associated proteins were detected by immunoblotting. (D) PANC-1 cells were treated with 3 μmol/L Sec C for the indicated time points, and proteins were determined by immunoblotting. (E) PANC-1 and AsPC-1 cells were treated with Sec C for 10 h, and lipid droplets were stained by BODIPY following fluorescence detection with a confocal microscope. Scale bar, 20 μm. (F) MIA PaCa2 cells were treated with different concentrations of Sec C for 10 h, and mRNA levels of key enzymes of lipid droplet formation were detected by real-time PCR. (G) MIA PaCa2 cells were transfected with BIP siRNA for 24 h prior to the addition of 3 μmol/L Sec C, and proteins at the indicated time points were detected by immunoblotting. The data are shown as mean ± SEM ($n = 3$); $^{*}P < 0.05$, $^{**}P < 0.01$, $^{***}P < 0.001$ *vs.* 0 μmol/L group.

3.2. Sec C induces mitochondria-mediated apoptosis in GEM-R and GEM-S pancreatic cancer cells

To further explore the anticancer mechanism of Sec C and to determine whether the mechanism was similar in GEM-S and GEM-R cells, we carried out the following assays. We first examined apoptosis and found that Sec C could induce it, and the number of apoptotic cells increased with increasing drug concentrations for both GEM-S BxPC-3 cells and GEM-R MIA PaCa2 cells (Fig. 2A). Correspondingly, we detected apoptosis-

associated proteins (cleaved PARP and cleaved caspase 3) and found that their expression increased in dose-dependent (Fig. 2B and Supporting Information Fig. S2A) and time-dependent (Fig. 2C and Fig. S2B) manners with treatment. All these apoptosis-related results were observed in GEM-S and GEM-R cells, indicating that a similar death mechanism was induced by Sec C in both types of cells.

Then, we examined whether Sec C-induced apoptosis was mediated by mitochondria. Generally, when mitochondria are damaged, cytochrome *c* is released to trigger a series of caspase reactions leading to apoptosis. We isolated the cytoplasm and mitochondria to determine the distribution of cytochrome *c* and found that cytoplasmic cytochrome *c* levels increased significantly with treatment, while mitochondrial cytochrome *c* levels decreased; these findings indicated that cytochrome *c* was released into the cytoplasm from the mitochondria after Sec C administration (Fig. 2D and Fig. S2C).

In addition, we detected mitochondrial membrane potential with JC-1 dye by flow cytometry (Fig. 2E) and fluorescence microscopy (Fig. 2F and Fig. S2D). The results show that the mitochondrial membrane potential in Sec C-treated cells was significantly lower than the mitochondrial membrane potential in control cells. Meanwhile, we observed that the expression of PUMA, an apoptosis-promoting protein, was increased in a dose-dependent manner (Fig. 2G and Fig. S2E). All the above-mentioned results demonstrate that Sec C induces apoptosis in a mitochondria-mediated manner.

3.3. *Sec C induces ER stress and lipid droplet formation in GEM-R and GEM-S pancreatic cancer cells*

In our electron microscopy assays, aside from swelling and vacuolization of mitochondria, we also found considerable enlargement and vacuolization of ER in Sec C-treated cells (Fig. 3A), suggesting that Sec C treatment might have damaged the ER and caused it to lose its primary structure. We transfected cells with YFP-ER plasmid, which labels the ER lumen, and a GFP-Sec61β plasmid, which labels the ER membrane, to further examine ER changes. The results showed that ER vacuoles and ER reticular structures were present in both YFP-ER and GFP-Sec61β cells at the lower dose of 1−2 μmol/L (Fig. 3B).

The ER is a cellular organelle that is critical for protein folding, secretion and lipid biosynthesis. When unfolded and misfolded proteins increase, ER stress is initiated. Then, ER stress sensors activate PERK/EIF2α/ATF4[23] and the ER stress-associated protein BIP (a chaperone that assists in proper protein folding). Following exposure to Sec C, we observed that PERK−EIF2α−ATF4 pathway (Fig. 3C and Supporting Information Fig. S3A) and IRE1α−XBP1 (Fig. S3B) pathway were activated, and the activated levels of PERK−EIF2α−ATF4 pathway were higher than the activated levels of IRE1α−XBP1 pathway. But there was no activation effect observed in ATF 6 pathway (Fig. S3B). The expression of ATF4 target gene BAX increased and BCL2 expression decreased (Fig. 3D and Fig. S3C). Meanwhile as the downstream molecular of activated IRE1, JNK was phosphorylated (Fig. S3B).

We also observed considerable numbers of lipid droplets in Sec C-treated cells in electron microscopy images. As reported in a previous review[24], the ER participates in lipid biosynthesis, and ER stress can induce lipid metabolic disorder, leading to the formation of lipid droplets. Thus, we hypothesized that the lipid droplet formation induced by Sec C might be a result of ER stress. We applied the fluorescent lipid probe BODIPY to quantify lipid droplets. The results showed that the numbers of lipid droplets obviously increased in a dose-dependent manner with treatment (Fig. 3E and Fig. S3D).

To clarify the cause of lipid droplet formation, we detected the levels of key lipogenic regulators/enzymes that can promote lipid droplet formation and can be induced by pharmacological ER stress according to previous reports[24]. These regulators/enzymes included mainly *FSP27*, *FIT2*, and *AP2*. The results reveal that the mRNA levels of *FSP27*, *FIT2* and *AP2* all increased with increasing Sec C concentrations (Fig. 3F), indicating that Sec C could induce key ER stress-associated lipogenic regulator or enzyme expression increase and subsequently promote lipid droplet formation. All the above results demonstrated that Sec C could induce severe ER damage to disturb lipid metabolism and subsequently activate the ER stress pathway.

ER stress initiation usually leads to two effects: when ER stress is mild, the stress-activated pathway can restore ER homeostasis by promoting unfolded or misfolded protein degradation; alternatively, when stress is strong, activation of the PERK−EIF2−ATF4 pathway enhances the expression of ATF4 target genes such as BAX and correspondingly decreases the expression of BCL2. BAX and BCL2 expression changes increase mitochondrial permeability to promote the release of cytochrome *c* from mitochondria into the cytoplasm, triggering apoptosis[25].

In our study, we observed that Sec C activated the ER stress pathway and ER-associated proteins, increased BAX levels, and induced cytochrome *c* release and apoptosis. Thus, we speculated that Sec C-mediated activation of the ER stress response and upregulation of ER-associated proteins facilitated cytochrome *c* release, thereby activating apoptosis.

The chaperone BIP is one of the most abundant proteins within the ER. During the ER stress-induced UPR, BIP was upregulated as a primary and direct ER stress sensor[26−28], and BIP was an essential regulator of the UPR pathway[29,30]. In our study, BIP was upregulated in a time-dependent manner in response to Sec C-induced UPR; thus, to further validate the role of BIP in ER stress and the role of ER stress in apoptotic induction in presence of Sec C, we knocked down BIP, and results show that BIP depletion attenuated the ER stress response and rescued the increase of pro-apoptosis proteins (Fig. 3G and Fig. S3E), indicating a diverse role of BIP in ER stress induction from some reports (BIP has a negative effect on ER stress induction)[31−33] and that Sec C induced ER stress to subsequently lead to the upregulation of the ATF4 target gene BAX and downregulation of BCL2 to enhance mitochondrial permeability, which induced cytochrome *c* release and apoptosis.

3.4. *Microarray and gene set enrichment analysis*

To further investigate the molecular pathway involved in Sec C activity, we treated AsPC-1, MIA PaCa2 and PANC-1 cells with Sec C and a solvent control. After RNA extraction and RNA-seq analysis, we performed Gene Set Enrichment Analysis using gene sets for oncogenic pathways in the Molecular Signature Database[34]. The results reveal that the UPR and apoptosis pathways were significantly enriched after Sec C treatment (Fig. 4A), in line with our data mentioned above.

Then, we analyzed the DEGs in each treated cell *vs.* control cell and found that the number of DEGs for every comparison exceeded 1000. Upon comparing and integrating the transcriptomic data, we found 239 overlapping DEGs among the 3

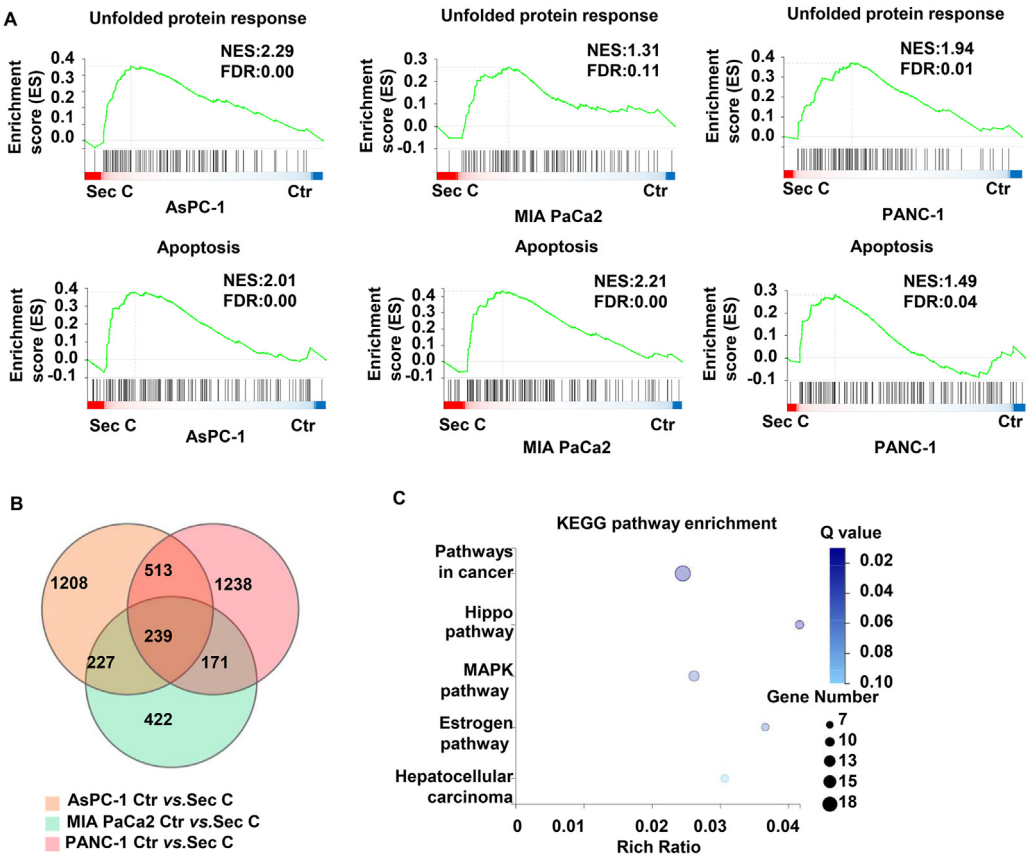

Figure 4 Microarray and gene set enrichment analysis. (A) AsPC-1, MIA PaCa2 and PANC-1 cells were treated with 3 μmol/L Sec C for 12 h, RNA was extracted for RNA-seq analysis with microarray, and Gene Set Enrichment Analysis in the Molecular Signature Database was performed. (B) Venn diagram of DEGs from 3 comparisons (treatment *vs*. control for AsPC-1 cells, MIA PaCa2 cells and PANC-1 cells). |log2 Ritio| $\geq$ 1, FDR value $\leq$ 0.001. (C) Oncogenic pathway functional enrichment of 239 DEGs from the 3 abovementioned comparisons.

comparisons (treatment *vs*. control for AsPC-1 cells, MIA PaCa2 cells and PANC-1 cells) (FDR $<$ 0.001, |Fold changes|$\geq$2) (Fig. 4B). KEGG pathway enrichment analysis showed that these 239 DEGs were significantly enriched in many pathways (Fig. 4C). Among the cancer pathways, the Hippo signaling pathway was the most obviously enriched for the DEGs. That is, numerous well-characterized TAZ/YAP target genes were found to be downregulated in the RNA-seq dataset in Sec C-treated group (data not shown), indicating that YAP activity was decreased and the Hippo signaling pathway was inhibited.

3.5. YAP participates in Sec C-mediated ER stress and apoptosis

The abovementioned RNA-seq results showed that *YAP* transcriptional activity was decreased; thus, we further observed *YAP* mRNA levels based on an RNA-seq assay. To our surprise, we did not observe a change in the *YAP* mRNA level, and therefore, we hypothesized that YAP protein regulation might influence YAP activity. Then, we detected *YAP* mRNA levels by real-time PCR and protein levels after Sec C administration. In accordance with the RNA-seq data, *YAP* mRNA levels did not obviously change (Fig. 5A), but YAP protein levels decreased significantly in both MIA PaCa2 and PANC-1 cells (Fig. 5B). To further ascertain the role of YAP in Sec C-induced ER stress and subsequent apoptosis, we overexpressed YAP prior to the addition of Sec C and detected whether the growth inhibition, ER stress and subsequent apoptosis induced by Sec C were reversed. A colony formation assay verified that overexpression of YAP reversed Sec C-induced growth inhibition (Fig. 5C). To further verify the role of YAP, we transfected cells with an inactive YAP mutant (S127D) and an active YAP mutant (S127A), and an inactive mutant (S127D) could not reverse Sec C-induced anticancer effect (Fig. 5E and Fig. S4B), while the active mutant (S127A) exerted an effect similar to the effect of wild-type YAP (Fig. 5D and Supporting Information Fig. S4A). These results demonstrate that Sec C-induced YAP downregulation contributed to ER stress and subsequent apoptosis to exert an anticancer effect in both GEM-S and GEM-R cells. Previous data showed that YAP played a positive role in ER stress triggering and that the PERK kinase−EIF2α axis regulated YAP. These data are different from our data regarding the role of YAP, revealing a unique role of YAP in ER stress.

3.6. Sec C induces YAP degradation via ER stress-mediated protein ubiquitylation and degradation

The abovementioned results demonstrate that Sec C treatment did not obviously decrease *YAP* mRNA levels but did decrease YAP protein levels, indicating that Sec C-induced YAP downregulation might be a result of increased YAP protein degradation (decreased stability). To further verify our hypothesis, cells were treated with CHX to block YAP protein synthesis before being exposed to Sec

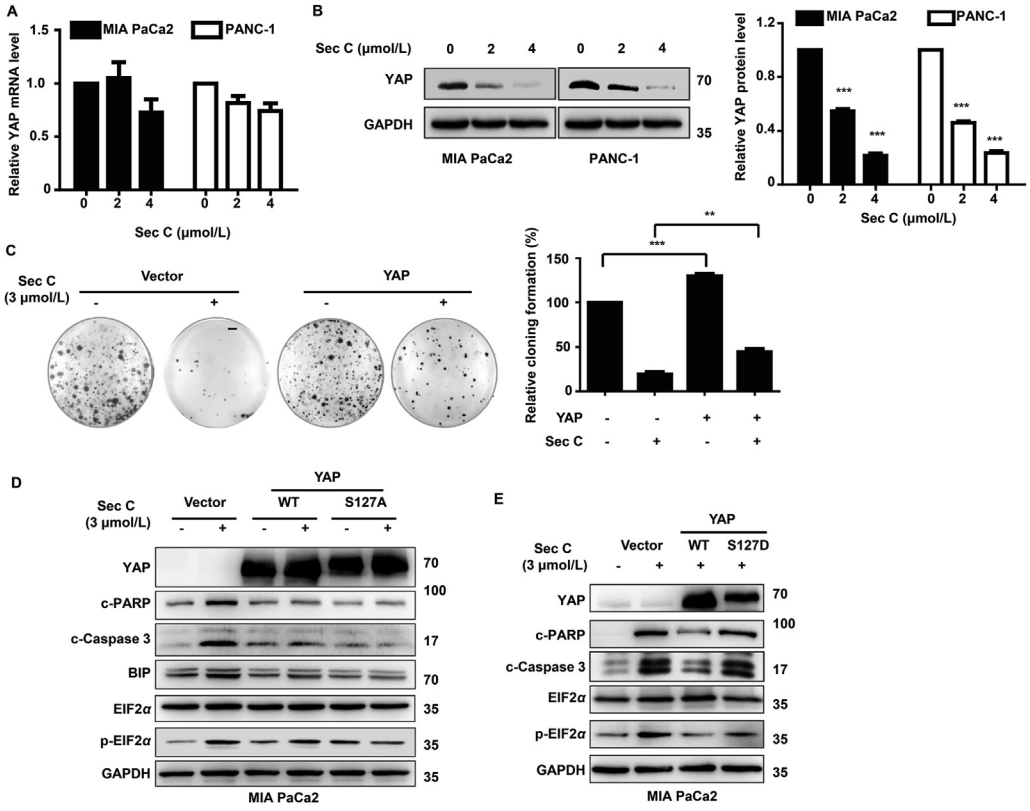

Figure 5 YAP participates in Sec C-mediated ER stress apoptosis. (A) MIA PaCa2 and PANC-1 cells were treated with Sec C for 12 h, YAP mRNA was detected by real-time PCR, and YAP protein was detected by immunoblotting (B). ***$P < 0.001$ *vs.* 0 μmol/L group. (C) MIA PaCa2 cells were transfected with YAP for 24 h followed by the addition of Sec C (3 μmol/L) for 7 days, and colony numbers were counted. Scale bar, 3 mm. Data are shown as mean ± SEM ($n = 3$); *$P < 0.05$, **$P < 0.01$, ***$P < 0.001$ *vs.* untreated group. (D) MIA PaCa2 cells were transfected with YAP, YAPS127A or vector followed by the addition of Sec C (3 μmol/L) for 12 h, and the indicated proteins were detected by immunoblotting. (E) MIA PaCa2 cells were transfected with YAP, YAPS127D or vector followed by the addition of Sec C (3 μmol/L) for 12 h, and the indicated proteins were detected by immunoblotting.

C to observe whether the YAP level was still decreased without a synthesized change in YAP. The results reveal that YAP protein levels were still decreased and that the half-life of YAP was shortened from 12 to 6 h (Fig. 6A), suggesting that Sec C promoted YAP protein degradation. There are two protein degradation pathways: the proteasome degradation pathway and the lysosomal degradation pathway. To ascertain which pathway was involved in YAP degradation induced by Sec C, the proteasome inhibitor MG132 and the lysosomal degradation inhibitor BAF were added to cells to determine which inhibitor could reverse Sec C-mediated YAP degradation. The results indicated that MG132, but not BAF, inhibited YAP degradation (Fig. 6B), suggesting that Sec C promoted YAP protein degradation *via* the proteasome degradation pathway. Among the proteasome degradation systems, the ubiquitin-mediated protein degradation pathway is the dominant pathway. Thus, we next detected YAP ubiquitination levels and found that YAP ubiquitination was indeed increased; these results showed that Sec C promoted YAP ubiquitination to initiate YAP degradation (Fig. 6C and Supporting Information Fig. S5A).

Protein ubiquitination is a process in which ubiquitin ligases transfer ubiquitin to a target protein for proteasomal degradation. In the final step of protein ubiquitination, E3 ubiquitin ligases specifically recognize protein substrates and transfer ubiquitin to proteins. Our results reveal that YAP ubiquitination was elevated; thus, we detected the binding between YAP and its specific E3 ligase β-TrCP and found that it was strengthened in the presence of Sec C (Fig. 6C). Previous research on YAP stability has focused on the YAP phosphorylation site at Ser397; Ser397 phosphorylation can promote the binding between YAP and β-TrCP. Therefore, we examined phosphorylated YAP (Ser397) levels but did not observe any increases. Rather, the phosphorylated YAP (Ser397) levels were decreased (Fig. 6D and Fig. S5B), indicating that phosphorylation of YAP at Ser397 was not the cause of the increased binding between YAP and its E3 ligase. Recent reports have shown that the formation of a YAP destruction complex containing the Axin, GSK3β, YAP and YAP E3 ubiquitin enzymes β-TrCP contributes to the binding of YAP and β-TrCP and subsequent YAP ubiquitination[35]. Thus, we examined the effect of Sec C on the formation of this destruction complex, and the results show that Sec C potentiated destruction complex formation (Fig. 6E and Fig. S5C), explaining the increase in YAP ubiquitination.

In response to ER stress, ER-associated degradation, also named ER stress-induced protein ubiquitylation and degradation, usually plays a key role in the maintenance of ER homeostasis[36]. During this process, incorrectly folded or unfolded proteins are dislocated into the cytosol for ubiquitylation with ubiquitin ligases for degradation *via* proteasomal activity[37–39]. In Sec C-treated

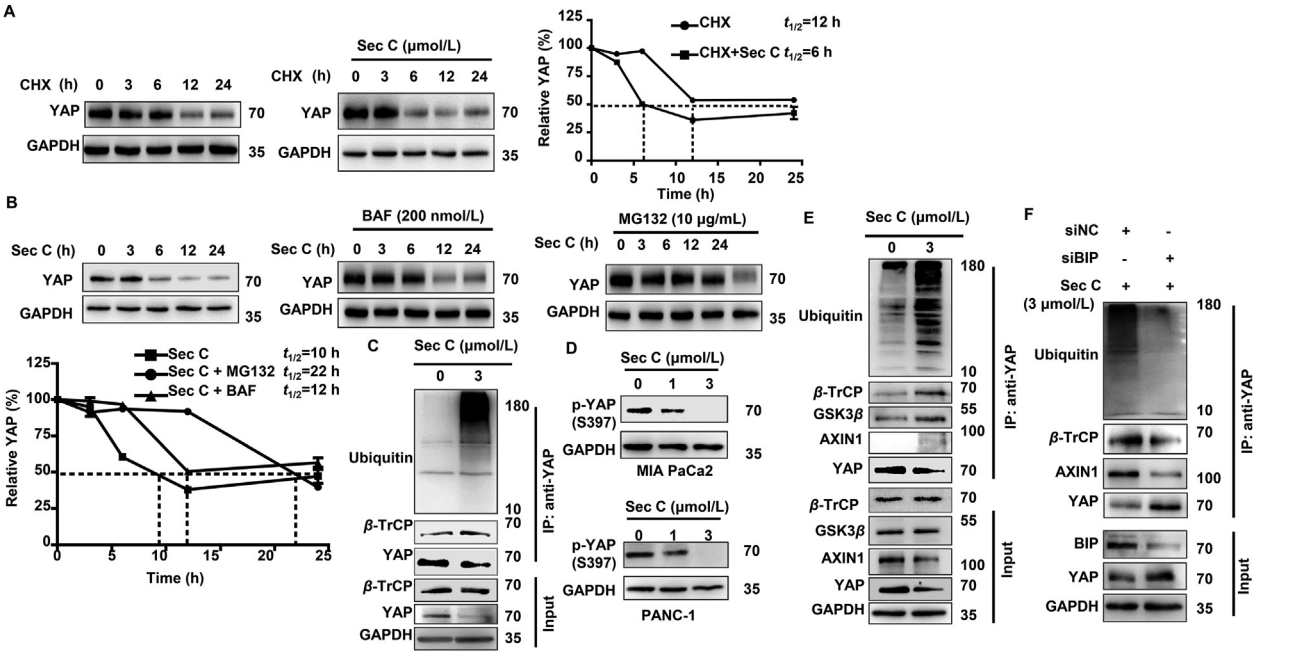

Figure 6 Sec C induces YAP degradation *via* ERAD-induced protein ubiquitylation and degradation. (A) MIA PaCa2 cells were treated with CHX (10 μg/mL) in the presence or absence of Sec C for the indicated time, and the YAP protein was examined. (B) MIA PaCa2 cells were treated with Sec C (3 μmol/L) or a combination of Sec C (3 μmol/L) and MG132 (10 μmol/L)/BAF (200 nmol/L) for the indicated time points, and the YAP protein was detected by immunoblotting. The data are shown as mean ± SEM (n = 3). (C) MIA PaCa2 cells were treated with Sec C (3 μmol/L) for 24 h, and YAP was immunoprecipitated for ubiquitin detection by immunoblotting. (D) MIA PaCa2 cells and PANC-1 cells were treated with different concentrations of Sec C for 24 h, and phosphor-YAP (Ser397) was determined by immunoblotting. MIA PaCa2 cells were treated in the absence (E) or presence of siBIP (F) prior to the addition of Sec C (3 μmol/L), cell extracts were immunoprecipitated with anti-YAP antibody, and destructive complex associated proteins were detected by immunoblotting.

cells, we observed that YAP was ubiquitylated and ER stress was activated; thus, we speculated that ER stress-induced protein ubiquitylation and degradation triggered YAP ubiquitylation and further degradation. To clarify this issue, we performed further assays to evaluate whether YAP ubiquitylation and degradation could be restored when ER stress was abrogated, and the results showed that the decrease in YAP and ubiquitylation were restored when ER stress was reduced (Fig. 6F). These results demonstrated that ubiquitination and degradation of YAP in Sec C-treated cells was mediated by ERAD in GEM-R cells, and in ERAD induction the different role of BIP from some reports[40,41].

3.7. *Knockdown of YAP sensitizes cells to the anticancer activity of compounds*

The above results reveal that overexpression of YAP abrogated Sec C-induced anticancer effects, indicating that YAP might be a resistance gene. Previous reports have revealed that YAP is overexpressed in many human cancers and that it is a transcriptional coactivator that promotes the expression of pro-proliferative and antiapoptotic genes[42–52]. Using the Gene Expression Profiling Interactive Analysis (GEPIA) tool, we found that the YAP levels in pancreatic cancer patients were significantly higher than the YAP levels in normal subjects (Fig. 7A). Further analysis revealed that the survival rate of the high-YAP group was significantly lower than the survival rate of the low-YAP group (Fig. 7B).

To further validate the resistant role of YAP in pancreatic cancer, we knocked down YAP in MIA PaCa2 cells prior to treating the cells with GEM and Sec C, and cell survival was analyzed. The results revealed that, consistent with the results that overexpression of YAP counteracted the inhibitory effects of anticancer agents (Fig. 5C); knockdown of YAP also enhanced the anticancer effects (Fig. 7C).

3.8. *Sec C sulfates cysteines in ER proteins to disturb formation of disulfide-bonds in ER proteins to trigger ER stress*

Sec C contains a bridged 4-sulfide piperazine ring. Our previous data on compounds containing similar bridged sulfides and reports by others have revealed that bridged sulfides are the essential active moieties of anticancer agents[53,54]. Furthermore, a previous investigation revealed that compounds containing sulfur atoms can form mixed disulfide bonds with reduced SH of cysteine residues to disrupt thiol proteostasis to inhibit cancer growth[54]. Research has shown that the organelle ER is the dominant site containing abundant cysteine residues[18,55]. Considering the bridged sulfide of Sec C, the abundance of cysteine in the ER and the potent ER stress effect mediated by Sec C, we hypothesized that Sec C might sulfurate ER cysteine to form disulfide-bonds to interrupt thiol proteostasis and induce the UPR effect. Although there is another amino acid methionine containing S, due to its structure, it hardly forms disulfide bonds with other amino acids[56].

To further ascertain that Sec C might form disulfide bonds with cysteine, we performed the following assays. First, we introduced NAC into our assay. NAC, a well-established cysteine derivative, can break disulfide bonds or replace cysteine residues in proteins to exert its reducing activity and thus is used to determine whether disulfide bonds are formed[57,58]. And results show that in the presence of Sec C, NAC could abrogate Sec C-induced ER stress, and the subsequent apoptosis (Fig. 8A and B, and Supporting

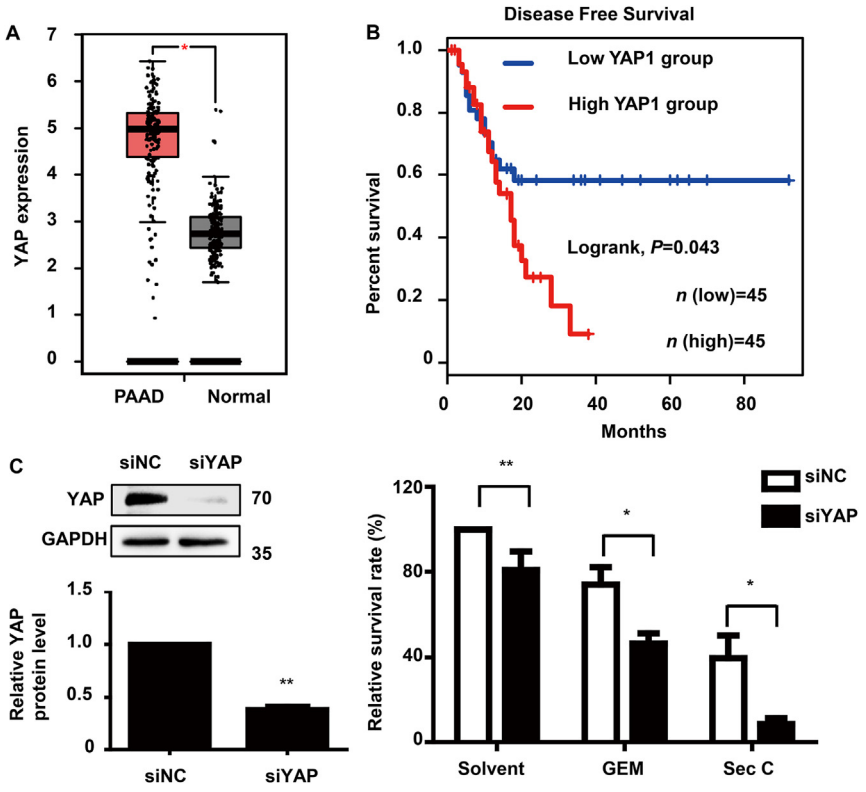

Figure 7 Knockdown of YAP sensitizes PAAD cells to the anticancer activity of compounds. (A) YAP expression in pancreatic cancer patients and normal tissues from GEPIA. (B) Disease-free survival of patients based on YAP expression. Kaplan−Meier curves were constructed to observe the survival of patients with high and low YAP expression. Patients with YAP expression within the top 75% were chosen as the high YAP group, and those with YAP expression in the bottom 1/4 were chosen as the low YAP group. Differences were evaluated by a log-rank (Mantel−Cox) test ($n = 90$; 45 high YAP expression patients and 45 low YAP expression patients) (GEPIA). (C) MIA PaCa2 cells were transfected with si*YAP* and control siNC for 24 h followed by the addition of GEM (2 μmol/L), Sec C (2 μmol/L) or solvent for 24 h, and cell vitality was determined by MTT assay. The data are shown as mean ± SEM ($n = 3$). $^{*}P < 0.05$, $^{**}P < 0.01$, $^{***}P < 0.001$ (C left: $^{**}P < 0.01$ *vs*. siNC group).

Information Fig. S6A), indicating that Sec C might form disulfide-bonds with protein.

Then, to further affirm that Sec C mainly sulfureted cysteine in ER proteins, we extracted ER and whole cell lysates and conducted a dBrB assay in which dBrB could react with free reduced thiols (SH) of cysteine to generate a highly fluorescent protein−dBrB adduct by detecting the content of the protein−dBrB adduct to verify the reaction ability of the compound and SH[59,60]. Through detection of SH of cysteine in the ER with a dBrB assay, we identified whether Sec C could decrease ER SH levels. Correspondingly, we also added NAC to Sec C-treated cells to detect whether NAC could reverse Sec C-induced decrease in ER SH levels. The positive control iodoacetamide (IAM) was used, and it can react with cysteine-SH groups to form stable *S*-carboxyaminodimethyl−cysteine adducts[60,61]. Results turned out IAM treatment and Sec C all effectively reduced the free cysteine-SH levels of ER in MIA PaCa2 cells (Fig. 8C), and the decrease in cysteine-SH levels induced by Sec C was dose-dependent. Moreover, NAC addition restored Sec C-induced decrease in cysteine-SH.

The SH content of whole cell lysate was also detected, and the results showed that the degree of decrease of SH level in whole cell lysate was 5 times less than the degree of decrease of SH level in ER extraction, indicating that Sec C could primarily decrease ER SH levels and form stable adducts with ER proteins containing SH. Finally, we used ER lysates to further identify Sec C−cysteine adducts by LC−MS/MS. The proteins from ER extraction lysates were subjected to trypsinization with specific endonuclease. Then, these tryptic peptides were sequenced by online microcapillary LC−MS/MS operated in a data-dependent mode and identified using the Byonic program. Next, the peptides were cleaved at different sites to ascertain which amino acid was bound to Sec C. This method to identify adducts is similar to the method used to identify phosphorylation sites in peptides (in which amino acids are phosphorylated[62]). As displayed in Fig. 8D, we observed that the cysteine residues of many peptides were bound to Sec C. For instance, we found that the molecular weight of the TCMYR peptide increased by 662 (the molecular weight of Sec C is 662), indicating that the drug was bound to the peptide. Then, through second-grade sequencing of the ion peaks y1, y2 and b1, we found that the increased molecular weight was not present in the C-terminal R (arginine) and Y (tyrosine) residues or the N-terminal T (threonine) residue but was associated with C (cysteine), indicating that Sec C was bound to C (cysteine). Based on the disulfide bond formation requirements and the bridged 4-sulfide piperazine ring structure of Sec C, we hypothesize that there are two binding styles between Sec C and cysteine. In one style, the bridged 4-sulfide piperazine ring of Sec C is opened, and one sulfur atom of Sec C forms a disulfide-bonds with the sulfur atom of the cysteine residue, resulting in an increase in

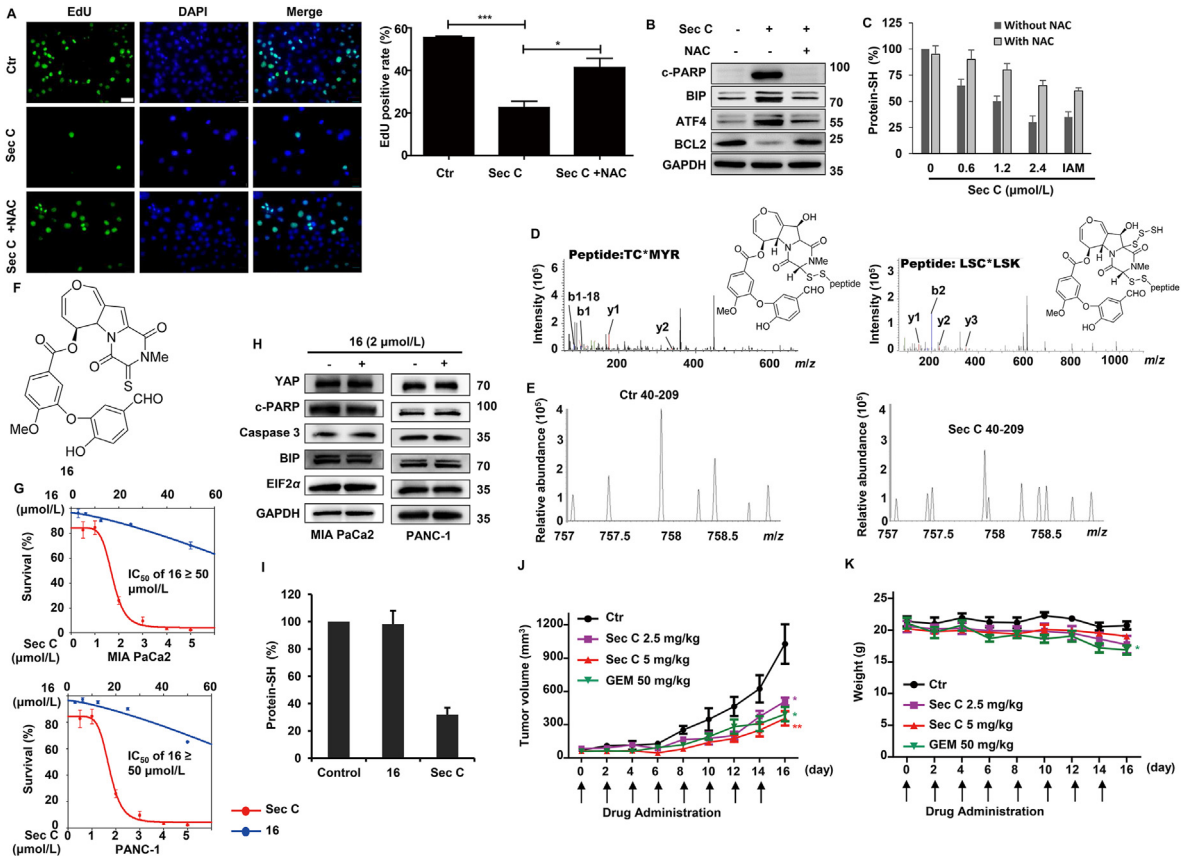

Figure 8 Sec C sulfates cysteines in ER proteins to disturb disulfide bond formation in ER proteins to trigger ER stress. MIA PaCa2 cells were treated with Sec C (2 μmol/L) in the absence or presence of NAC (25 μmol/L) for 24 h, and cell vitality was detected with EdU assay (A). Proteins were detected by immunoblotting (B), and ER proteins were extracted for thiol group detection by dBrB assay (C). MIA PaCa2 cells were treated with Sec C (2 μmol/L) for 24 h, the ER fraction was extracted, and Sec C−protein binding sites (D) and disulfide-bonds of ER proteins (E) were analyzed *via* LC−MS/MS. The peptides were identified as TC*MYR and LSC*LSK (C: cysteine; *: binding site of Sec C in the peptide). (F) Structure of compound **16**. (G) MIA PaCa2 or PANC-1 cells were treated with compound **16** for 48 h, and the IC_{50} was calculated. MIA PaCa2 or PANC-1 cells were treated with compound **16** (2 μmol/L) for 24 h, and then proteins were extracted for Western blot detection (H) and SH protein detection by dBrB assay (I). The data are shown as mean ± SEM ($n = 3$). Nude mice bearing GEM-R MIA PaCa2 cells were administered Sec C on Day 8 after tumor inoculation and successively administered Sec C every second day. Mice were sacrificed when the tumor volume of the control group reached 1000 mm. The tumor volume (mm^3) (J) and body weight (K) were monitored and plotted. The data are shown as mean ± SEM ($n = 5$). $^*P < 0.05$, $^{**}P < 0.01$, $^{***}P < 0.001$. Scale bar, 40 μm.

the molecular weight of the peptide by 662 (the compound has a molecular weight of 662), as shown in the left plot in Fig. 8D. In the other style, the bridged 4-sulfide piperazine ring is opened, Sec C loses 3 sulfur atoms, and the remaining sulfur atom combines with the sulfur atom in the cysteine residue to form a disulfide bond, resulting in an increase in the molecular weight of the peptide by 566. As shown in the right plot in Fig. 8D, the molecular weight of the LSCLSK peptide increased by 566, and further observation of the ion peaks y1, y2, y3 and b2 indicated that the increase in molecular weight was not in the C-terminal K (lysine), L (leucine) or S (serine) residues or in the N-terminal L and S residues, only C (cysteine) and Sec C could be combined.

As reported[63–65], disulfide-bonds plays a required and key role during correct folding of ER proteins. Deregulation of disulfide-bonds formation can lead to the accumulation of misfolded proteins and ER stress induction[66–68], and inhibition of PDI (protein disulfide isomerase which could promote disulfide-bonds formation) could induce ER stress and the unfolded protein response[69]. To further verify whether the disulfide-bonds formed between Sec C and ER cysteines interfered with the formation of disulfide-bonds in ER proteins which is essential for correct protein folding. We further detected the content of disulfide-bonds in ER proteins in Sec C-treated cells *via* LC−MS/MS, and the results show that the content of disulfide-bonds decreased, suggesting that Sec C inhibited the formation of disulfide-bonds thus ER stress and subsequent apoptosis were induced (Fig. 8E). Furthermore, NAC (a cysteine analog) addition reversed the sulfation of ER proteins and thus reversed ER stress, and apoptosis was restored, further verifying the anticancer mechanism of Sec C mentioned above (Fig. 8C).

Meanwhile, we introduced a constructive analog of Sec C, compound **16** (Fig. 8F), whose structure is analogous to Sec C with the exception of bridged sulfides, to further elucidate the effect of bridged sulfides on ER stress, YAP levels and anticancer activity. The results showed that the IC_{50} of compound **16** exceeded 50 μmol/L, but in the same cell line, the IC_{50} of Sec C was only approximately 1 μmol/L (Fig. 8G). Moreover, at the same concentration at which Sec C induced ER stress, apoptosis and YAP decrease in two cell lines, we did not observe ER stress, apoptosis and YAP decrease in addition of **16** (Fig. 8H and

Fig. S6B), nor did we observe the binding between compound and cysteine residues (Fig. 8G), indicating that bridged sulfide-induced sulfation in ER protein plays the key role in ER stress, apoptosis and anticancer exhibition.

Then, we evaluated the anticancer efficacy of Sec C *in vivo* by transplanting GEM-R MIA PaCa2 cells into nude mice. The results indicated that Sec C could suppress tumor xenograft proliferation. At 5 mg/kg, the inhibitory rate was approximately 71%, while at 2.5 mg/kg, the inhibitory rate was approximately 55% (Fig. 8J). The body weight curves indicated that the animals tolerated the administered Sec C doses well (Fig. 8K). We also applied GEM (50 mg/kg, much higher than the dose of Sec C) to GEM-R cells as a positive control and found that although 50 mg/kg GEM could exhibit an anticancer effect, obvious decreases in body weight occurred, suggesting strong toxicity in the GEM-treated group with GEM-R cell transplantation. These data show that Sec C exhibits an excellent inhibitory effect on GEM-R pancreatic cancer cells without causing obvious toxicity *in vivo*.

4. Discussion

Natural products have been vital sources for the discovery of anticancer drugs. From 1981 to date, approximately 34% of the drugs approved by the FDA have been made from natural products and their derivatives; these natural products have been derived mostly from microbes and plants and have usually served as skeleton compounds[70]. The diversity of pharmacophores and the complexity of the spatial configuration of natural products facilitate the binding of these natural products to their targets, which subsequently improves screening accuracy[71]. Another advantage of natural products over synthetic compounds is that natural products have metabolite-like characteristics that allow them to "hitchhike" through transporters of endogenous metabolites to enter target cells, increasing their bioavailability[72–75]. Thus, exploration of natural products has been an important aspect of drug discovery and development.

Sec C, a natural product from microbes, was originally isolated in 1997 from metabolites of the fungi *Emericella striata* and *Emericella quadrilineata*. Since 1997, the biological activities of Sec C, including its anticancer activity, have not been explored. Our research reveals that Sec C could exert potent anticancer effects in both GEM-S and GEM-R pancreatic cancer cells. The IC_{50} of GEM was above 60 μmol/L in GEM-R cells, but the IC_{50} of Sec C was 2−4 μmol/L in these cells, similar to the IC_{50} in GEM-S pancreatic cancer cells, suggesting that Sec C can inhibit cancer growth regardless of GEM resistance.

Our findings also revealed another beneficial effect of Sec C: although Sec C and GEM have a similar IC_{50} in GEM-S cells, Sec C could kill 80% of cancer cells following 6 h of administration at 1.5-fold the IC_{50}, and at the same concentration, GEM only inhibited 20% of the cell proliferation. These findings indicate that Sec C can rapidly kill tumor cells, which is very important for some tumor patients. Usually, preoperative shrinkage of tumors *via* chemotherapy is essential to prevent tumor invasion during surgery. However, for some tumor patients who urgently need tumor resection surgery (for example, due to tumor rupture or compression of vital organs), rapid shrinkage of tumors is especially important. The rapid cell-killing effects of Sec C will aid in shrinking tumors quickly in such cases. Furthermore, the rapid action of Sec C may help prevent further spread of tumors and reduce the duration of postoperative drug therapy.

We further investigated why there were no differences in Sec C-mediated anticancer effects between GEM-S and GEM-R cells and why Sec C could rapidly exhibit anticancer effects. A mechanistic study showed that Sec C could bind ER proteins in GEM-R and GEM-S cells and form disulfide bonds with these proteins, which interfered with their normal functions and led to folding and modification failure in some ER proteins. These effects led to the accumulation of unfolded or misfolded proteins, and ER stress was induced. Continued ER stress activated the PERK−EIF2α−ATF4 pathway, which then increased the expression of the ATF target gene BAX, leading to an increase in mitochondrial membrane permeability and ultimately to mitochondria-mediated apoptosis. Notably, the ER, which is the target of Sec C, is enriched in pancreatic tissues compared to other tissues, especially in pancreatic cancer tissues, and ER chaperone proteins that enhance ER stress are also highly expressed regardless of GEM resistance. Furthermore, the resistance gene YAP was found to play an essential role in Sec C-induced anticancer activity in GEM-R and GEM-S cells; thus, Sec C exhibited potent antitumor effects irrespective of GEM resistance.

In our study, we found that Sec C downregulated YAP protein levels to activate Sec C-triggered ER stress pathway and subsequently increased ER damage-induced mitochondrial membrane permeability. However, diverse opinions have been presented about the mechanism by which YAP regulates ER stress, and the relationship between YAP and the UPR is convoluted and seems to be more complicated than other stresses. In one study[76], tauroursodeoxycholic acid, a hydrophilic bile acid derivative, was found to alleviate ER size-associated ER stress and downregulate YAP; further exploration revealed that tauroursodeoxycholic acid alleviated ER stress by downregulating YAP and that YAP played a positive role in triggering ER stress. In addition, the same study reported that prolonged ER stress-induced Hippo signaling inhibited YAP expression in a negative feedback loop and promoted apoptosis and demonstrated that the PERK kinase−EIF2α axis regulates YAP. Another report revealed that suberoylanilide hyroxamic acid inhibits YAP activity to activate ER stress and promote survival in differentiating muscle and sarcoma cells[77]. These data are different from our data regarding the role of YAP. For instance, in our study, YAP expression was decreased following Sec C treatment, ER stress was induced to trigger cell death, and YAP inhibited ER stress and negatively regulated the PERK kinase−EIF2α axis. We hypothesize that the different roles of YAP in ER stress activation might be due to the diverse types of ER damage induced by the various agents. These diverse types of ER damage might initiate other corresponding pathways that might affect the role of YAP in ER stress. Our research reveals a novel role of YAP in ER stress induction and shows that YAP might exhibit multiple functions in various cells in response to treatment with diverse compounds.

5. Conclusions

Sec C, a natural anticancer compound produced by endophytic fungi, exhibits excellent anticancer effects against GEM-R/GEM-S cells and will be a beneficial treatment for patients with primary and secondary GEM resistance. In addition, the rapid action of Sec C compared with GEM will enable rapid assistance for patient's urgently needing surgery. As Sec C is a fungal metabolite, its production is scalable, low-cost and pollution-free. These characteristics make Sec C a promising drug for the treatment of

pancreatic cancer. The unique mechanism of Sec C, including degradation of YAP to enhance ER stress *via* promotion of YAP destruction complex formation, also provides new ideas for the development of antitumor drugs.

Acknowledgments

This work was supported by the National Key Research and Development Program of China (2016YFA0201504), National Natural Science Foundation of China (No. 81473249 and 81102464), the National Mega-project for Innovative Drugs (2014ZX09201042, China), the CAMS Innovation Fund for Medical Sciences (CIFMS, 2016-I2M-2-002, China) and Drug Innovation Major Project of China (2018ZX09711001-007-002).

Author contributions

Rongguang Shao, Shuyi Si and Wuli Zhao contributed to the experimental design; Wuli Zhao, Minghua Chen, Junxia Wang and Xiujun Liu and the other authors contributed to data acquisition and analysis; Rongguang Shao reviewed the manuscript; Wuli Zhao and Rongguang Shao obtained the funding; and Wuli Zhao and Junxia Wang wrote the manuscript.

Conflicts of interest

The authors declare no conflicts of interest.

Appendix A. Supporting information

Supporting data to this article can be found online at https://doi.org/10.1016/j.apsb.2021.07.004.

References

1. He W, Wu J, Shi J, Huo YM, Dai W, Geng J, et al. IL22RA1/STAT3 signaling promotes stemness and tumorigenicity in pancreatic cancer. *Cancer Res* 2018;**78**:3293−305.
2. Carrato A, Falcone A, Ducreux M, Valle JW, Parnaby A, Djazouli K, et al. A systematic review of the burden of pancreatic cancer in Europe: real-world impact on survival, quality of life and costs. *J Gastrointest Cancer* 2015;**46**:201−11.
3. Zhou J, Zhang L, Zheng H, Ge W, Huang Y, Yan Y, et al. Identification of chemoresistance-related mRNAs based on gemcitabine-resistant pancreatic cancer cell lines. *Cancer Med* 2020;**9**:1115−30.
4. Burris 3rd HA, Moore MJ, Andersen J, Green MR, Rothenberg ML, Modiano MR, et al. Improvements in survival and clinical benefit with gemcitabine as first-line therapy for patients with advanced pancreas cancer: a randomized trial. *J Clin Oncol* 1997;**15**:2403−13.
5. Jia C, Jiachun Y, Vijaya R, Thiruvengadam A, Defeng D, Zhaoshen L, et al. TM4SF1 promotes gemcitabine resistance of pancreatic cancer *in vitro* and *in vivo*. *PLoS One* 2015;**10**:e0144969.
6. Yoshida K, Toden S, Ravindranathan P, Han H, Goel A. Curcumin sensitizes pancreatic cancer cells to gemcitabine by attenuating PRC2 subunit EZH2, and the lncRNA PVT1 expression. *Carcinogenesis* 2017;**38**:1036−46.
7. Réjiba S, Bigand C, Parmentier C, Hajri A. Gemcitabine-based chemogene therapy for pancreatic cancer using Ad-dCK::UMK GDEPT and TS/RR siRNA strategies. *Neoplasia* 2009;**11**:637−50.
8. Bayraktar S, Bayraktar UD, Rocha-Lima CM. Recent developments in palliative chemotherapy for locally advanced and metastatic pancreas cancer. *World J Gastroenterol* 2010;**16**:673−82.
9. Ron D, Walter P. Signal integration in the endoplasmic reticulum unfolded protein response. *Nat Rev Mol Cell Biol* 2007;**8**:519−29.
10. Berridge MJ. The endoplasmic reticulum: a multifunctional signaling organelle. *Cell Calcium* 2002;**32**:235−49.
11. Martinon F. Targeting endoplasmic reticulum signaling pathways in cancer. *Acta Oncol* 2012;**51**:822−30.
12. Lee JS, Wu Y, Schnepp P, Fang J, Zhang X, Karnovsky A, et al. Proteomics analysis of rough endoplasmic reticulum in pancreatic beta cells. *Proteomics* 2015;**15**:1508−11.
13. Steiner DF. Adventures with insulin in the islets of Langerhans. *J Biol Chem* 2011;**286**:17399−421.
14. Arvan P. Secretory protein trafficking: genetic and biochemical analysis. *Cell Biochem Biophys* 2004;**40**:169−78.
15. Rozpedek W, Pytel D, Mucha B, Leszczynska H, Diehl JA, Majsterek I. The role of the PERK/eIF2alpha/ATF4/CHOP signaling pathway in tumor progression during endoplasmic reticulum stress. *Curr Mol Med* 2016;**16**:533−44.
16. Hetz C, Glimcher LH. Fine-tuning of the unfolded protein response: assembling the IRE1alpha interactome. *Mol Cell* 2009;**35**:551−61.
17. Kraskiewicz H, FitzGerald U. InterfERing with endoplasmic reticulum stress. *Trends Pharmacol Sci* 2012;**33**:53−63.
18. Seo MJ, Lee DM, Kim IY, Lee D, Choi MK, Lee JY, et al. Gambogic acid triggers vacuolization-associated cell death in cancer cells *via* disruption of thiol proteostasis. *Cell Death Dis* 2019;**10**:187.
19. Cragg GM, Newman DJ. Natural product sources of drugs: plants, microbes, marine organisms, and animals. In: Taylor JB, Triggle DJ, editors. *Comprehensive medicinal chemistry II*. Oxford: Elsevier Science; 2007. p. 355−403.
20. Ooike M, Nozawa K, Kawai KI. An epitetrathiodioxopiperazine related to emestrin from *Emericella foveolata*. *Phytochemistry* 1997;**46**:123−6.
21. Liu H, Zhao WL, Wang JP, Xin BM, Shao RG. EBP50 suppresses the proliferation of MCF-7 human breast cancer cells *via* promoting Beclin-1/p62-mediated lysosomal degradation of c-Myc. *Acta Pharmacol Sin* 2018;**39**:1347−58.
22. Okada M, Shi YB. Cell Proliferation analysis during xenopus metamorphosis: using 5-ethynyl-2-deoxyuridine (EdU) to stain proliferating intestinal cells. *Cold Spring Harb Protoc* 2017;**2017**:pdb.prot097717.
23. Long F, Yang D, Wang J, Wang Q, Liu X. SMYD3−PARP16 axis accelerates unfolded protein response and mediates neointima formation. *Acta Pharm Sin B* 2021;**11**:1261−73.
24. Jacquemyn J, Cascalho A, Goodchild RE. The ins and outs of endoplasmic reticulum-controlled lipid biosynthesis. *EMBO Rep* 2017;**18**:1905−21.
25. Jurgensmeier JM, Xie Z, Deveraux Q, Ellerby L, Bredesen D, Reed JC. Bax directly induces release of cytochrome *c* from isolated mitochondria. *Proc Natl Acad Sci U S A* 1998;**95**:4997−5002.
26. Bakunts A, Orsi A, Vitale M, Cattaneo A, Lari F, Tade L, et al. Ratiometric sensing of BiP-client *versus* BiP levels by the unfolded protein response determines its signaling amplitude. *Elife* 2017;**6**:e27518.
27. Kopp MC, Larburu N, Durairaj V, Adams CJ, Ali MM. UPR proteins IRE1 and PERK switch BiP from chaperone to ER stress sensor. *Nat Struct Mol Biol* 2019;**26**:1053−62.
28. Adams CJ, Kopp MC, Larburu N, Nowak PR, Ali MM. Structure and molecular mechanism of ER stress signaling by the unfolded protein response signal activator IRE1. *Front Mol Biosci* 2019;**6**:11.
29. Chapman R, Sidrauski C, Walter P. Intracellular signaling from the endoplasmic reticulum to the nucleus. *Annu Rev Cell Dev Biol* 1998;**14**:459−85.
30. Okamura K, Kimata Y, Higashio H, Tsuru A, Kohno K. Dissociation of Kar2p/BiP from an ER sensory molecule, Ire1p, triggers the unfolded protein response in yeast. *Biochem Biophys Res Commun* 2000;**279**:445−50.
31. Samanta S, Yang S, Debnath B, Xue D, Kuang Y, Ramkumar K, et al. The hydroxyquinoline analogue YUM70 inhibits GRP78 to induce ER stress-mediated apoptosis in pancreatic cancer. *Cancer Res* 2021;**81**:1883−95.

32. Kuo CY, Lin CH, Hsu T. VHL Inactivation in precancerous kidney cells induces an inflammatory response *via* ER stress-activated IRE1α signaling. *Cancer Res* 2017;**77**:3406−16.
33. Fu Y, Li J, Lee AS. GRP78/BiP inhibits endoplasmic reticulum BIK and protects human breast cancer cells against estrogen starvation-induced apoptosis. *Cancer Res* 2007;**67**:3734−40.
34. Subramanian A, Tamayo P, Mootha VK, Mukherjee S, Ebert BL, Gillette MA, et al. Gene set enrichment analysis: a knowledge-based approach for interpreting genome-wide expression profiles. *Proc Natl Acad Sci U S A* 2005;**102**:15545−50.
35. Azzolin L, Panciera T, Soligo S, Enzo E, Bicciato S, Dupont S, et al. YAP/TAZ incorporation in the beta-catenin destruction complex orchestrates the Wnt response. *Cell* 2014;**158**:157−70.
36. Kwon D, Kim SM, Correia MA. Cytochrome P450 endoplasmic reticulumassociated degradation (ERAD): therapeutic and pathophysiological implications. *Acta Pharm Sin B* 2020;**10**:42−60.
37. Lee MC, Miller EA, Goldberg J, Orci L, Schekman R. Bi-directional protein transport between the ER and Golgi. *Annu Rev Cell Dev Biol* 2004;**20**:87−123.
38. Römisch K. Endoplasmic reticulum-associated degradation. *Annu Rev Cell Dev Biol* 2005;**21**:435−56.
39. Egger L, Madden D, Rheme C, Rao R, Bredesen D. Endoplasmic reticulum stress-induced cell death mediated by the proteasome. *Cell Death Differ* 2007;**14**:1172−80.
40. Hegde NR, Chevalier MS, Wisner TW, Denton MC, Shire K, Frappier L, et al. The role of BiP in endoplasmic reticulum-associated degradation of major histocompatibility complex class I heavy chain induced by cytomegalovirus proteins. *J Biol Chem* 2006;**281**:20910−9.
41. Wang M, Wey S, Zhang Y, Ye R, Lee AS. Role of the unfolded protein response regulator GRP78/BiP in development, cancer, and neurological disorders. *Antioxid Redox Signal* 2009;**11**:2307−16.
42. Yi C. Downstream of mutant KRAS, the transcription regulator YAP is essential for neoplastic progression to pancreatic ductal adenocarcinoma. *Sci Signal* 2014;**4**:ra42.
43. Sudol M, Bork P, Einbond A, Kastury K, Druck T, Negrini M, et al. Characterization of the mammalian YAP (Yes-associated protein) gene and its role in defining a novel protein module, the WW domain. *J Biol Chem* 1995;**270**:14733−41.
44. Sudol M. Yes-associated protein (YAP65) is a proline-rich phosphoprotein that binds to the SH3 domain of the Yes proto-oncogene product. *Oncogene* 1994;**9**:2145−52.
45. Kanai F, Marignani PA, Sarbassova D, Yagi R, Yaffe MB. TAZ: a novel transcriptional co-activator regulated by interactions with 14-3-3 and PDZ domain proteins. *Embo J* 2000;**19**:6778−91.
46. Yagi R, Chen LF, Shigesada K, Murakami Y, Ito Y. A WW domain-containing Yes-associated protein (YAP) is a novel transcriptional co-activator. *EMBO J* 1999;**18**:2551−62.
47. Vassilev A, Kaneko KJ, Shu H, Zhao Y, DePamphilis ML. TEAD/TEF transcription factors utilize the activation domain of YAP65, a Src/Yes-associated protein localized in the cytoplasm. *Genes Dev* 2001;**15**:1229−41.
48. Justice RW, Zilian O, Woods DF, Noll M, Bryant PJ. The *Drosophila* tumor suppressor gene warts encodes a homolog of human myotonic dystrophy kinase and is required for the control of cell shape and proliferation. *Genes Dev* 1995;**9**:534−46.
49. Harvey KF, Pfleger CM, Hariharan IK. The *Drosophila* Mst ortholog, *hippo*, restricts growth and cell proliferation and promotes apoptosis. *Cell* 2003;**114**:457−67.
50. Wu S, Huang J, Dong J, Pan D. *Hippo* encodes a Ste-20 family protein kinase that restricts cell proliferation and promotes apoptosis in conjunction with *salvador* and *warts*. *Cell* 2003;**114**:445−56.
51. Tapon N, Harvey KF, Bell DW, Wahrer DCR, Schiripo TA, Haber DA, et al. *Salvador* Promotes both cell cycle exit and apoptosis in *Drosophila* and is mutated in human cancer cell lines. *Cell* 2002;**110**:467−78.
52. Lai ZC, Wei X, Shimizu T, Ramos E, Rohrbaugh M, Nikolaidis N, et al. Control of cell proliferation and apoptosis by Mob as tumor suppressor, Mats. *Cell* 2005;**120**:675−85.
53. Wang F, Zhao W, Zhang C, Chang S, Shao R, Xing J, et al. Cytotoxic metabolites from the endophytic fungus *Chaetomium globosum* 7951. *RSC Adv* 2019;**9**:16035−9.
54. Gardiner DM, Gardiner DM, Waring P, Howlett BJ. The epipolythiodioxopiperazine (ETP) class of fungal toxins: distribution, mode of action, functions and biosynthesis. *Microbiology* 2005;**151**:1021−32.
55. Bechtel TJ, Li C, Kisty EA, Maurais AJ, Weerapana E. Profiling cysteine reactivity and oxidation in the endoplasmic reticulum. *ACS Chem Biol* 2020;**15**:543−53.
56. Ruoppolo M, Vinci F, Klink TA, Raines RT, Marino G. Contribution of individual disulfide bonds to the oxidative folding of ribonuclease A. *Biochemistry* 2000;**39**:12033−42.
57. Aldini G, Altomare A, Baron G, Vistoli G, Carini M, Borsani L, et al. *N*-Acetylcysteine as an antioxidant and disulphide breaking agent: the reasons why. *Free Radic Res* 2018;**52**:1−12.
58. Balsamo R, Lanata L, Egan CG. Mucoactive drugs. *Eur Respir Rev* 2010;**19**:127−33.
59. Rudyk O, Eaton P. Biochemical methods for monitoring protein thiol redox states in biological systems. *Redox Biol* 2014;**2**:803−13.
60. Zanotto-Filho A, Masamsetti VP, Loranc E, Tonapi SS, Gorthi A, Bernard X, et al. Alkylating agent induced NRF2 blocks endoplasmic reticulum stress-mediated apoptosis *via* control of glutathione pools and protein thiol homeostasis. *Mol Cancer Ther* 2016;**15**:3000−14.
61. Anderson PJ, Perham RN. The reactivity of thiol groups and the subunit structure of aldolase. *Biochem J* 1970;**117**:291−8.
62. Guo L, Kozlosky CJ, Ericsson LH, Daniel TO, Johnson RS. Studies of ligand-induced site-specific phosphorylation of epidermal growth factor receptor. *J Am Soc Mass Spectrom* 2003;**14**:1022−31.
63. Wallis AK, Freedman RB. Assisting oxidative protein folding: how do protein disulphide-isomerases couple conformational and chemical processes in protein folding?. *Top Curr Chem* 2013;**328**:1−34.
64. Camacho CJ, Thirumalai D. Modeling the role of disulfide bonds in protein folding: entropic barriers and pathways. *Proteins* 1995;**22**:27−40.
65. Robinson PJ, Pringle MA, Woolhead CA, Bulleid NJ. Folding of a single domain protein entering the endoplasmic reticulum precedes disulfide formation. *J Biol Chem* 2017;**292**:6978−86.
66. Medinas DB, Rozas P, Martinez Traub F, Woehlbier U, Brown RH, Bosco DA, et al. Endoplasmic reticulum stress leads to accumulation of wild-type SOD1 aggregates associated with sporadic amyotrophic lateral sclerosis. *Proc Natl Acad Sci U S A* 2018;**115**:8209−14.
67. Welker E, Wedemeyer WJ, Scheraga HA. A role for intermolecular disulfide bonds in prion diseases?. *Proc Natl Acad Sci U S A* 2001;**98**:4334−6.
68. Torres M, Medinas DB, Matamala JM, Woehlbier U, Cornejo VH, Solda T, et al. The protein-disulfide isomerase ERp57 regulates the steady-state levels of the prion protein. *J Biol Chem* 2015;**290**:23631−45.
69. Ozcelik D, Seto A, Rakic B, Farzam A, Supek F, Pezacki JP. Gene expression profiling of endoplasmic reticulum stress in hepatitis C virus-containing cells treated with an inhibitor of protein disulfide isomerases. *ACS Omega* 2018;**3**:17227−35.
70. Patridge E, Gareiss P, Kinch MS, Hoyer D. An analysis of FDA-approved drugs: natural products and their derivatives. *Drug Discov Today* 2016;**21**:204−7.
71. Harvey AL, Edrada-Ebel R, Quinn RJ. The re-emergence of natural products for drug discovery in the genomics era. *Nat Rev Drug Discov* 2015;**14**:111−29.
72. Palikaras K, Lionaki E, Tavernarakis N. Coordination of mitophagy and mitochondrial biogenesis during ageing in *C. elegans*. *Nature* 2015;**521**:525−8.

73. Kell DB. Implications of endogenous roles of transporters for drug discovery: hitchhiking and metabolite-likeness. *Nat Rev Drug Discov* 2016;**15**:143.
74. Dobson PD, Patel Y, Kell DB. 'Metabolite-likeness' as a criterion in the design and selection of pharmaceutical drug libraries. *Drug Discov Today* 2009;**14**:31−40.
75. Lee YH, Choi H, Park S, Lee B, Yi GS. Drug repositioning for enzyme modulator based on human metabolite-likeness. *BMC Bioinf* 2017;**18**:226.
76. Wu H, Wei L, Fan F, Ji S, Zhang S, Geng J, et al. Integration of Hippo signalling and the unfolded protein response to restrain liver overgrowth and tumorigenesis. *Nat Commun* 2015; **6**:6239.
77. Paraskevi K, Rand JD, Weids AJ, Wang X, Kershaw CJ, Grant CM. ER stress-induced reactive oxygen species (ROS) are detrimental for the fitness of a thioredoxin reductase mutant. *J Biol Chem* 2018;**293**: 11984−95.